OXFORD UNIVERSITY PRESS | Cerebral Cortex

Genome-Wide Transcriptional Profiling and Structural Magnetic Resonance Imaging in the Maternal Immune Activation Model of Neurodevelopmental Disorders

Journal:	*Cerebral Cortex*
Manuscript ID	Draft
Manuscript Type:	Original Articles
Date Submitted by the Author:	n/a
Complete List of Authors:	Richetto, Juliet; University of Zurich-Vetsuisse, Institute of Pharmacology and Toxicology; ETH Zurich, Physiology and Behavior Laboratory Chesters, Robert; King\'s College London, Department of Basic and Clinical Neuroscience, Institute of Psychiatry Psychology and Neuroscience Cattaneo, Annamaria; IRCCS Fatebenefratelli San Giovanni di Dio, Biological Psychiatry Laboratory; King\'s College London, Stress, Psychiatry and Immunology Laboratory, Department of Psychological Medicine, Institute of Psychiatry Wood, Tobias; King\'s College London, Department of Neuroimaging, Institute of Psychiatry Psychology and Neuroscience Gutierrez, Ana Maria Carillo; King\'s College London, Department of Basic and Clinical Neuroscience, Institute of Psychiatry Psychology and Neuroscience Luoni, Alessia; University of Milan, Department of Pharmacological and Biomolecular Sciences Meyer, Urs; University of Zurich - Vetsuisse, Institute for Pharmacology and –toxicology Vernon, Anthony; King\'s College London, Department of Basic and Clinical Neuroscience, Institute of Psychiatry Psychology and Neuroscience Riva, Marco; University of Milan, Department of Pharmacological and Biomolecular Sciences
Keywords:	Magnetic resonance imaging (MRI), maternal immune activation, poly(I:C), schizophrenia, transcriptome

Genome-Wide Transcriptional Profiling and Structural Magnetic Resonance Imaging in the Maternal Immune Activation Model of Neurodevelopmental Disorders

Juliet Richetto[1,2,§], Robert Chesters[3,§], Annamaria Cattaneo[4,5], Ana Maria Carrillo Gutierrez[3], Tobias C. Wood[6], Alessia Luoni[7], Urs Meyer[1,2,*], Anthony Vernon[3,#], Marco A. Riva[7#]

[1]Institute of Pharmacology and Toxicology, University of Zurich-Vetsuisse, Zurich, Switzerland.
[2]Physiology and Behavior Laboratory, ETH Zurich, Schwerzenbach, Switzerland.
[3]Department of Basic and Clinical Neuroscience, Institute of Psychiatry Psychology and Neuroscience, King's College London, London, UK.
[4]Biological Psychiatry Laboratory, IRCCS Fatebenefratelli San Giovanni di Dio, Brescia, Italy.
[5]Stress, Psychiatry and Immunology Laboratory, Department of Psychological Medicine, Institute of Psychiatry, King's College London, London, UK.
[6]Department of Neuroimaging, Institute of Psychiatry Psychology and Neuroscience, King's College London, London, UK.
[7]Department of Pharmacological and Biomolecular Sciences, Università degli Studi di Milano, Milan, Italy.

[§]These authors corresponded equally to the present study.
[#]Shared seniority.

*Correspondence:
Urs Meyer, Ph.D.
Institute of Pharmacology and Toxicology
University of Zurich-Vetsuisse
Winterthurerstrasse 260,
8057 Zurich, Switzerland

E-mail: urs.meyer@vetpharm.uzh.ch
Tel.: +41 44 635 88 44; Fax.: +41 44 635 89 10

Running Title: Prenatal Infection and Myelination-Related Deficits.

Key Words: Magnetic resonance imaging (MRI); maternal immune activation; myelin; poly(I:C); schizophrenia; transcriptome.

Abstract

Prenatal exposure to maternal infection can increase the risk of neuropsychiatric disorders with neurodevelopmental components, including schizophrenia and autism. The molecular processes underlying this pathological association, however, are only partially understood. Here, we combined unbiased genome-wide transcriptional profiling with follow-up epigenetic analyses and structural magnetic resonance imaging to explore convergent molecular and neuromorphological alterations in cortiostriatal areas of adult offspring exposed to prenatal viral-like immune activation. Genome-wide transcriptional profiling revealed that prenatal immune activation caused a differential expression of 116 and 251 genes in the medial prefrontal cortex and nucleus accumbens, respectively. A large part of genes that were commonly affected in both brain areas were related to myelin functionality and stability. Subsequent epigenetic analyses indicated that DNA hypermethylation of promoter regions underlies the differential expression of myelin-related genes. Quantitative relaxometry comparing T_1, T_2 and myelin water fraction revealed consistent reductions in T_2 (but not T_1) relaxation times. Together, our multi-systems approach demonstrates that prenatal viral-like immune activation causes myelin-related transcriptional and epigenetic changes in cortiostriatal areas. Even though these abnormalities do not seem to be associated with overt white matter reduction, they may provide a molecular mechanism whereby prenatal infection can impair myelin functionality and stability.

Introduction

The aetiology of multifactorial and multi-symptomatic neuropsychiatric disorders likely includes exposures to adverse events during prenatal and early postnatal life, which may disrupt the development and maturation of neural systems and brain functions (Brown AS 2011). Prenatal exposure to infectious or inflammatory insults is increasingly recognized to play an important role in this context. Indeed, immune-related prenatal adversities have been repeatedly linked with a higher risk of neurodevelopmental psychiatric disorders, including schizophrenia, and autism, and bipolar disorder (Brown AS and EJ Derkits 2010; Patterson PH 2011; Marangoni C et al. 2016). These epidemiological associations are further supported by translational work in animal models demonstrating abnormal brain development and behavioural dysfunctions following prenatal administration of infectious pathogens or immune activating agents (Meyer U and J Feldon 2010; Harvey L and P Boksa 2012; Meyer U 2014).

The advances in modelling prenatal immune activation effects in animals hold promise for the identification of pathological mechanisms that translate the prenatal insult into long-term brain abnormalities. The majority of these experimental attempts, however, have thus far been hypothesis-driven and focused on the role of a specific cellular or molecular mechanism, pathway or system (Eyles D et al. 2012; Ibi D and K Yamada 2015). While this is a laudable and possibly fruitful approach for the examination of a presumed pathophysiological mechanism, it may be prone to an overestimation of the relative importance of a given effect. Such *a priori* assumptions may also distract from the discovery of novel mechanisms that may contribute to the emergence of long-term brain abnormalities following prenatal immune challenges.

The implementation of genome-wide transcriptional profiling is one possible approach to overcome these limitations. It allows an unbiased screen of gene expression changes in response to prenatal immune activation, which can form the basis for follow-up investigations that take into account this transcriptomic information (Tebbenkamp AT et al. 2014; Horvath S and K Mirnics 2015). Fatemi and colleagues were the first to investigate the effects of prenatal infection with influenza virus on global transcription in mouse models (Fatemi SH et al. 2005; Fatemi SH et al. 2008; Fatemi SH, TD Folsom, TJ Reutiman, D Abu-Odeh, et al. 2009; Fatemi SH, TD Folsom, TJ Reutiman, H Huang, et al. 2009). This pioneering work identified transcriptomic changes in numerous genes implicated in schizophrenia and other psychiatric disorders, which were detectable in various brain regions such as the cortex, hippocampus, and cerebellum (Fatemi SH et al. 2005; Fatemi SH et al. 2008; Fatemi SH, TD Folsom, TJ Reutiman, D Abu-Odeh, et al. 2009; Fatemi SH, TD Folsom, TJ Reutiman, H Huang, et al. 2009). A number of subsequent studies have then used microarray techniques to explore genome-wide transcriptomic abnormalities in foetal (Oskvig DB et al. 2012) or adult (Connor CM et al. 2012) offspring prenatally exposed to a viral-like acute phase response. Overall, these studies provided support for the hypothesis that prenatal viral infection or viral-like immune activation can cause short- and long-term changes in gene expression with relevance to neurodevelopmental disorders. The wide array of information provided by these transcriptomic analyses, however, was only partly considered as a starting point for follow-up investigations that could help translating the observed gene expression changes into neurobehavioral and -morphological abnormalities.

The present study sought to explore the consequences of prenatal immune activation by pursuing a multi-systems approach. Specifically, unbiased transcriptomic profiling formed the basis for subsequent focussed immunohistochemical investigations, and epigenetic analyses. Genome-wide transcriptomic profiling was performed using unbiased microarray techniques in the medial prefrontal cortex (mPFC) and nucleus accumbens (NAc), two brain regions implicated in neurodevelopmental disorders such as schizophrenia and autism (Richey JA et al. 2015; Schubert D et al. 2015; Selemon LD and N Zecevic 2015). The inclusion of two brain regions allowed us to identify region-specific and -overlapping transcriptomic effects of prenatal immune activation using a within-subjects comparison. These investigations were performed in offspring that were first subjected to behavioural and cognitive testing. In addition, we explored whether these micro scale alterations reverberate to influence macroscale alterations that are detectable using clinically comparable MR imaging. Specifically, we acquired anatomical scans for group-wise comparison of brain volume and utilised a novel putatively myelin-specific MRI technique (mcDESPOT) to provide quantitative information about proton tissue water relaxation times and myelin water fraction signals (Deoni SC et al. 2011). For this purpose, a separate cohort of behaviourally naïve animals underwent *ex vivo* MRI followed by *post-mortem* investigations guided by the MRI findings (Vernon AC et al. 2014). Advantages of this approach include that the examination of possible transcriptomic, epigenetic and neuroanatomical effects takes place against the background of overt behavioural and cognitive phenotypes, which appears particularly important for (immune-mediated) neurodevelopmental disruption models that may contain a certain degree of litter-to-litter variability (Meyer U et al.

2009). Furthermore, changes in macroscale MRI signals following gestational exposure to Poly (I:C) may be mapped to their microscale cellular correlates.

All investigations were performed using a well-established mouse model of prenatal viral-like immune activation. The model is based on maternal administration of the viral mimetic poly(I:C) (= *polyriboinosinic-polyribocytidilic acid*), which induces a cytokine-associated viral-like acute phase response in maternal and foetal compartments, including the foetal brain (Meyer U *et al.* 2009). Prenatal poly(I:C) treatment in rodents has repeatedly been shown to cause multiple behavioural and cognitive disturbances in the offspring, many of which are implicated in developmental psychiatric disorders such as schizophrenia and autism (Meyer U et al. 2009; Meyer U and J Feldon 2010; Harvey L and P Boksa 2012; Meyer U 2014). The poly(I:C) administration model thus offers a unique opportunity to explore genome-wide transcriptomic changes following prenatal exposure to an etiologically relevant risk factor, and to further link such changes with neurobehavioral and MRI-detectable abnormalities.

Materials and Methods

Animals

C57Bl6/N mice were used throughout the study. Female and male mice were originally obtained from Charles River Laboratories (Germany) and kept in our in-house specific-pathogen-free (SPF) facility until breeding began to generate poly(I:C)-exposed and control offspring (see below). All animal breeding and holding rooms were temperature- and humidity-controlled (21 ± 1 °C, 55 ± 5%) and kept under a reversed light–dark cycle (lights off: 7:00 A.M. to 7:00 P.M.). All animals had *ad libitum* access to food (Kliba 3430, Kaiseraugst, Switzerland) and water throughout the entire study. All procedures described in the present study had been previously approved by the Cantonal Veterinarian's Office of Zurich, and all efforts were made to minimize the number of animals used and their suffering.

Maternal Immune Activation during Pregnancy

Female C57Bl6/N mice were subjected to a timed mating procedure as described previously (Meyer U et al. 2005). Pregnant dams on gestation day (GD) 17 were randomly assigned to receiving either a single injection of poly(I:C) (potassium salt; Sigma–Aldrich, Buchs, St. Gallen, Switzerland) or vehicle. Poly(I:C) (5 mg/kg; calculated based on the pure form of poly(I:C)) was dissolved in sterile pyrogen-free 0.9% NaCl (vehicle) solution to yield a final concentration of 1 mg/ml and was administered intravenously (i.v.) into the tail vein under mild physical constraint. The dose of poly(I:C) was selected based on previous dose-response studies (Meyer U et al. 2005). 10 pregnant dams were injected with poly(I:C), and another 10 with vehicle solution.

With respect to reproductive and developmental biology in humans, the selected gestational window (i.e., GD 17) corresponds roughly to the beginning of the second trimester of human pregnancy (Clancy B et al. 2007). It was selected based on previous studies showing that prenatal poly(I:C) exposure during this gestational period causes adult behavioral, cognitive, and neuroanatomical abnormalities relevant to neurodevelopmental brain disorders, including schizophrenia and autism (Meyer U et al. 2006; Meyer U et al. 2008; Bitanihirwe BK, D Peleg-Raibstein, et al. 2010; Bitanihirwe BK, L Weber, et al. 2010; Richetto J et al. 2013; Richetto J et al. 2014; Richetto J et al. 2015). We previously verified that poly(I:C) administration on GD 17 is effective in terms of eliciting cytokine-associated inflammatory response in maternal and fetal tissues (Meyer U *et al.* 2006).

Allocation of Offspring and Group Sizes

Offspring of poly(I:C)-treated dams (POL) and vehicle-exposed control offspring (CON) were weaned and sexed on postnatal day (PND) 21. Littermates of the same sex were caged separately and maintained in groups of 3 to 4 animals per cage. Only male animals were included in all experiments. A first cohort of CON and POL offspring was used for the assessment of behavioral functions, which was followed by *post-mortem* microarray analyses, validation of gene expression, and DNA methylation analyses (see below). A second cohort of offspring was used for *ex vivo* MRI imaging and subsequent *post-mortem* immunohistochemical analyses (see below). In both cohorts, 1 male offspring per litter was randomly selected for the investigations of interest in order to avoid litter effects (Zorrilla et al. 1997). This led to a group size of N = 10 offspring per prenatal treatment

condition in each cohort. The DNA methylation analyses were performed using a subset of offspring, with *N* = 5 offspring per prenatal treatment condition.

Behavioral Testing

CON and POL offspring of cohort 1 were subjected to behavioral testing when they reached early adulthood (12 weeks of age). The tests included paradigms assessing working memory, social approach behavior, and social recognition. These tests were selected based on their relevance to neurodevelopmental disorders with infectious and inflammatory components, including schizophrenia and autism (Meyer U et al. 2009; Peleg-Raibstein D et al. 2012). A detailed description of the test apparatuses and procedures is provided in the **Supplementary Information**. Each animal underwent all behavioral tests in the following order: (1) working memory test and (2) social approach and recognition test. A test-free resting period of 2 days was imposed between the two tests.

Collection of Brain Samples for Molecular Analyses

CON and POL offspring of cohort 1 killed by decapitation 10 days after completion of behavioural testing for the subsequent molecular analyses. The brains were rapidly extracted from the skull (within < 20 s) and placed on an ice-chilled plate. This was followed by preparing 1-mm coronal brain sections using razorblade cuts and subsequent micro-dissection of the brain areas of interest. We dissected the medial prefrontal cortex (mPFC, including anterior cingulate, prelimbic and dorsal parts of the infralimbic cortices; bregma: +2.3 to +1.3 mm) and the nucleus accumbens (NAc, including core and shell subregions; bregma +1.5 to +0.5 mm) as previously described (Bitanihirwe BK, D Peleg-Raibstein, et al. 2010). Brain

specimens were collected in 96-well microtiter plates kept on dry ice and allowed to freeze before storage at −80°C until further use.

DNA and RNA Isolation

Total DNA and RNA were isolated using the Qiagen AllPrep DNA and RNA Mini kit (Qiagen, Italy) as described in the **Supplementary Information**.

Microarray Analyses

Genome-wide gene expression analyses were performed using Affymetrix microarray assays (Mouse Gene 1.1 ST Array Strips on GeneAtlas platform), following the 3'IVT one cycle labelling as fully described in the **Supplementary Information**. All the raw data are accessible at the NCBI GEO depository (GEO accession number GSE77973). The data analysis was performed with Partek Genomics Suite (Partek, USA), version 6.6 (for details, see **Supplementary information**). Differentially expressed genes (DEGs) in POL offspring relative to CON offspring were identified by performing a linear contrast (POL versus CON). In this comparison, a maximum filter of $p < 0.05$ and a minimum absolute fold change cut-off of 1.2 were applied. The DEGs were loaded into Partek Genomics Suite and were clustered according to the Hierarchical Clustering function of Partek Genomics Suite. For this purpose, the data was normalized with standardization (each column mean is zero, and the standard deviation is scaled to one), and then multidimensional scaling with a Euclidian distance metric was performed on the normalized samples to allow visualization of the distance between them. To confirm that the overlapping changes were not due to random distribution, we performed the hyper-geometric test in R (p=5.765284e-14).

Subsequent validation of selected DEGs was performed by quantitative real-time PCR as described below.

Quantitative Real-Time RT-PCR Analyses

mRNA levels were quantified by TaqMan qRT-PCR (CFX384 real-time system, Bio-Rad Laboratories) using the iScript one-step RT-PCR kit for probes (Bio-Rad Laboratories) (see **Supplementary Information**). Relative target gene expression was calculated according to the 2(-Delta Delta C(T)) method. Probe and primer sequences of Claudin11 (Assay: Mm00500915_m1) were purchased from Life Technologies (Switzerland), while the custom designed probe and primer sequences used for MOBP, MOG, MAL and MAG are summarized in **Supplementary Table 1** and were purchased from Eurofins Genomics GmbH (Germany).

DNA Methylation Analysis

DNA methylation levels of the α-myelin-associated oligodendrocytic basic protein (MOBP) promoter region were quantified using the EpiTYPER assay. This technique detects and quantifies DNA methylation using base-specific cleavage and Matrix-Assisted Laser Desorption/Ionization Time-of-Flight (MALDI-TOF) mass spectrometry (Suchiman HE et al. 2015). Genomic DNA was treated and analyzed as fully described in the **Supplementary Information**.

Brain Sample Preparation for MRI

At 12 weeks of age, CON and POL offspring from the second cohort were deeply anesthetized with an overdose of Nembutal (Abbott Laboratories) and perfused transcardially with 0.9% NaCl, followed by 4% phosphate-buffered

paraformaldehyde (PFA) solution containing 15% picric acid (Giovanoli S et al. 2013). After perfusion, the animals were decapitated and the skin, lower jaw and ears were removed. The brain within the skull was incubated in 4% PFA overnight at +4°C and then shipped to King's College London the next day. Upon arrival, brain samples were transferred to 0.01M phosphate buffered saline containing and 0.05% sodium azide for at least 7 days prior to MR imaging.

MRI acquisition, Processing and Analysis

A 7T horizontal small bore magnet and (Agilent Technologies Inc. Santa Clara, USA) and a quadrature volume radiofrequency coil (39 mm internal diameter, Rapid Biomedical GmbH) were used for all MRI acquisitions. Fixed brain samples were placed securely up to four at a time in an MR-compatible holder and immersed in proton-free susceptibility matching fluid (Fluorinert^{TM} FC-70; Sigma-Aldrich, UK). The following MR images were acquired: T_2-weighted 3D Fast Spin-Echo (FSE) and a multi-component Driven Equilibrium Single Pulse Observation of T_1 and T_2 (mcDEPSOT) protocol with B1 correction. The latter consists of a Spoiled Gradient echo (SPGR), balanced Steady State Free Procession (bSSFP) and Actual Flip-angle imaging (AFI) scans (Deoni SC et al. 2013). The mcDESPOT protocol generates data to calculate parametric maps of T_1, T_2 and the myelin water fraction (MWF) for each animal (**Supplementary Figure 1**). Parameters for each scan are summarised in **Supplementary Table 3**. MR image processing and analysis were performed as fully described in the **Supplementary information**.

Group-level differences in MRI parameters (volume, T_1, T_2 and MWF) between CON and POL offspring were analysed voxel-wise across the whole-brain using permutation testing and threshold free cluster enhancement (TFCE) (Smith SM

and TE Nichols 2009; Winkler AM et al. 2014) at an uncorrected *p* value of 0.01. Multiple comparisons were controlled for using the false discovery rate (FDR) (Genovese CR et al. 2002) at $q = 0.05$..

Immunohistochemistry

After completion of all MRI, fixed brain tissues were processed for immunohistochemical analyses as described in the **Supplementary information.** Standard immunohistochemical procedures were implemented to stain for α-myelin basic protein (MBP; rabbit anti-MBP; Abcam, Cat no. ab7349; diluted 1:1000) and MOBP (rabbit anti-MOBP; Abcam, Cat no. ab203388; diluted 1:500) as fully described in the **Supplementary information.**

Threshold Image Analysis for Myelin Staining

Quantitative analyses of MBP and MOBP-positive staining were performed in the mPFC using unbiased threshold image analysis as described in the **Supplementary Information**. All post-processing and analysis was performed using ImageJ software (http://imagej.nih.gov/ij/). The percentage area of immunopositive pixels in each acquired image of the mPFC, from 4 consecutive sections, were averaged to give a single value per animal.

Statistical Analyses

All behavioural and RT-PCR were analysed using independent Student's *t* tests (two-tailed). Immunohistochemical analysis was conducted using a one-tailed Student's T-test, given the *a-priori* hypothesis based on the strong gene

expression data. Statistical significance was set at $p < 0.05$ for these analyses. Microarray and MRI data were analysed as described above. DNA methylation levels measured using EpiTYPER were analysed using repeated-measures analysis of variance (RM-ANOVA) followed by Fisher's least significant difference (FLSD) post-hoc comparisons whenever appropriate. All statistical analyses were performed using the statistical software SPSS (v22.0; IBM Corporation, Armonk, New York, USA).

Results

Prenatal immune activation induces deficits in working memory and social interaction

First, we aimed to ascertain the deleterious effects of prenatal immune activation on adult behavioral and cognitive functions. We found that POL offspring displayed impaired working memory as assessed using a spatial recognition memory test in the Y-maze (**Figure 1A**). In this test, the critical measure of working memory is the relative time spent in the novel (previously unexplored) arm during the choice phase. CON offspring displayed a noticeable preference towards the novel arm, indicating intact working memory in these groups (**Figure 1A**). In contrast, POL offspring exhibited a marked reduction ($p < 0.5$) in this measure and performed only at chance level (**Figure 1A**). There were no group differences with respect to the total distance moved (**Figure 1A**), indicating that the negative effects of prenatal immune activation on working memory are not confounded by possible differences in basal locomotor activity.

POL offspring also displayed impaired marked deficits in the social interaction test, in which they were first allowed to concomitantly explore an inanimate dummy

object and an unfamiliar live mouse (**Figure 1B**). During this phase of the test, CON offspring showed a clear preference (> 65%) for the live mouse versus the inanimate dummy object (**Figure 1B**). By contrast, POL offspring did not display such a preference (**Figure 1B**), indicating reduced sociability towards unfamiliar conspecifics. This led to a significant ($p < 0.001$) group difference in the percent time spent with the live mouse (**Figure 1B**).

To test social recognition memory, the inanimate dummy object was then replaced by another unfamiliar life mouse, and the relative exploration time between the previously explored and novel live mouse was measured. During this phase of the social interaction test, CON offspring showed a clear preference (> 65 %) for the novel mouse (**Figure 1B**). POL offspring did not display such a preference, leading to a significant ($p < 0.05$) group difference in the percent time spent with the novel mouse (**Figure 1B**). In both phases of the social interaction test, there were no group differences with respect to the total distance moved. Hence, prenatal immune activation leads to genuine deficits in social approach behavior and recognition memory behavior without concomitant effects on general exploratory behavior.

Prenatal immune activation alters the long-term transcription profile of the prefrontal cortex and nucleus accumbens

As shown in **Fig 2A**, which represents the hierarchical clustering of expression changes induced by prenatal infection with Poly(I:C), 116 genes were differentially expressed in the prefrontal cortex (fold change cut-off: ± 1.2; $p < 0.05$), while 251 were differentially expressed in the nucleus accumbens. Of the 116 genes that were differentially expressed in the prefrontal cortex, 55 were down-regulated and

61 were up-regulated (**Table 1 and 2**), while in the nucleus accumbens, 126 were down-regulated and 125 up-regulated (**Table 3 and 4**). Interestingly, many of these have been already associated with schizophrenia, such as adenosine 2a receptor (ADORA2a), apolipoprotein D (APOD), the dopamine receptors DRD2 and DRD3, forkhead box P2 (FOXP2), glutaminase (GLS), the glutamate receptor subunit GRIN2A, histone cluster 1 (HIST1H2BC), 5-hydroxytryptamine receptors (HTR1A, HTR2A, HTR4), oxytocin (OXT), solute carriers (SLC17A7), and, among others, vescicle-associated membrane protein 4 (VAMP4) (Butler MG et al. 2015).

Next, the genes affected in both brain areas were compared. As shown in **Fig. 2B**, the Venn diagram of the two brain areas highlighted 14 common genes, 11 of which are modulated in the same direction in both brain areas (**Fig 2B**). In particular, Poly(I:C) exposure affected the expression of six main genes involved in myelination, both in the prefrontal cortex and in the nucleus accumbens: myelin and lymphocyte protein (MAL), myelin-associated glycoprotein (MAG), myelin-associated oligodendrocytic basic protein (MOBP), myelin oligodendrocyte glycoprotein (MOG), claudin 11 (Cldn11) and myelin regulatory factor (Myrf). The first 5 of these, which were found to be down-regulated by Poly(I:C) in the gene array analysis, resulted decreased by the prenatal manipulation also when analysed with real-time qRT-PCR (**Fig 3A)**. Interestingly, these genes are implicated in a variety of biological processes and functions implicated in myelination, as demonstrated by Ingenuity Pathway analysis (**Fig 3B**). Statistical support for these observations was provided by Student's t-test that yielded a significant effect of prenatal treatment for all five targets investigated ($p< 0.05$, $p< 0.01$ or $p<0.001$).

Macroscale MRI phenotyping of adult offspring exposed to prenatal immune activation

Unbiased, brain-wide tensor based morphometry (TBM) analysis of the neuroanatomical MR images revealed clusters of significantly (q=0.05 FDR corrected) expanded voxels bilaterally in an area encompassing the anterior cingulate cortex (ACC) and the M1/M2 motor cortices in POL mice relative to CON animals (**Figure 4**). Additional, unilateral, right-lateralised focal expansions were also present in the forceps minor of the corpus callosum (FMI), dorsal striatum and focal left lateralised expansions in the medial parietal association cortex (MtPA) in POL mice relative to CON offspring (**Figure 4**). There were no statistically significant (q=0.05 FDR corrected) clusters of contracted voxels (**Figure 4**). However, at an exploratory threshold (p<0.01 uncorrected), in addition to the above-mentioned cortical changes, several sub-cortical regions show apparent bilateral clusters of decreased voxels, including the paraventricular thalamic nucleus (PVA) ventral posteromedial thalamic nucleus (VPM), medial geniculate nucleus (MGN), periaqueductal gray (PAG) and the 4th, 5th and 10th cerebellar lobules (**Figure 4**). We found no evidence for either ventricular enlargement or decreases in hippocampus volume at this time-point.

Whole-brain cluster analysis comparing T_1, T_2 and MWF parameters revealed no significant differences in T_1 (spin-lattice) relaxation time between saline and POL offspring, at q=0.05 FDR corrected (**Figure 5A, B**), even at an exploratory threshold of p<0.01 uncorrected (*data not shown*). In contrast, T_2 (spin-spin) relaxation times were significantly decreased (shortened) across multiple brain regions at q=0.05 FDR corrected (**Figure 5A, B**). Shortening of T_2 were

particularly prominent bilaterally in the prefrontal cortex (PFC), hypothalamus, thalamic nuclei, amygdala, hippocampal formation and cerebellum (**Figure 5B**). Shortening of T_2 therefore appears to overlap with regions of volumetric expansion in the cortex, and regions that contract (e.g. thalamus, cerebellum), or show no apparent volumetric changes (e.g. amygdala, hippocampus), sub-cortically. At q=0.05 (FDR corrected) there were no significant changes in the myelin water fraction (MWF) (**Figure 5B**).

Prenatal immune activation affects protein expression levels of MOBP, but not MBP, in the prefrontal cortex

Against the background of our numerous findings, we sought to verify whether the gene expression and MR-detectable changes we observed translate into, and stem from, differential protein expression. Thus, we analysed the levels of MBP, a major constituent of the myelin sheath, and MOBP, one of the candidates that emerged from our genome wide study, with immunohistochemistry focusing on the prefrontal cortex. Consistent with our gene expression study, there were no significant differences in the percentage area of MBP-immunoreactive pixels in the PFC of either saline or POL exposed offspring (**Figure 6A**). In contrast, the percentage area of MOBP-immunoreactive pixels was numerically reduced in the PFC of POL offspring, relative to saline controls ($p<0.05$, Cohens'd =0.961, **Figure 6B**). These data are illustrated by representative photomicrographs for MBP and MOBP (**Figure 6A and B**, respectively).

Prenatal immune activation alters the methylation profile of the MOBP promoter

We were further interested in examining whether epigenetic modifications may be a plausible mechanism that could translate the effects of prenatal infection into long-lasting transcriptomic changes. To test this hypothesis, we analyzed DNA methylation profiles of the MOBP promoter in the prefrontal cortex using the EpiTYPER technique, which detects and quantifies DNA methylation using MALDI-TOF mass spectrometry (Suchiman HE *et al.* 2015). We focused on MOBP because the initial microarray and subsequent RT-PCR analyses consistently revealed decreased expression of this myelination-related gene in offspring exposed to prenatal immune activation relative to control offspring (**Figure 2A and 3A**).

We found hypermethylation of multiple CpGs sites in two distinct MOBP promoter segments that are adjacent to (amplicon 1) or incorporate (amplicon 2) the transcriptional start site (TSS) (**Figure 7**). RM-ANOVA of percent methylation in amplicon 1 demonstrates a significant interaction between prenatal treatment and CpG site ($F_{(6,54)}$ = 5.35, p < 0.001), indicating that the infection-induced changes in CpG methylation levels differ as a function of genomic location. Indeed, post-hoc comparisons at each individual CpG site revealed increased (p < 0.05) methylation levels at CpG_{507} and CpG_{457} in POL compared to CON offspring, whereas decreased (p < 0.05) methylation levels at CpG_{343} were found in the former relative to the latter group (**Figure 7B,C**). On the other hand, the CpG sites encompassed in amplicon 2 were generally hypermethylated in POL relative to CON offspring (**Figure 7B,C**), as supported by the main effect of prenatal treatment in the RM-ANOVA of percent methylation ($F_{(1,9)}$ = 7.32, p < 0.05).

Discussion

The present study analysed the gene expression profile of the mPFC and NAc following exposure to late prenatal immune activation, and implemented a multi-systems approach based on MR imaging, immunohistochemistry and epigenetic analyses to follow up the gene expression changes it uncovered. Late prenatal immune activation led to the dysregulation of a variety of different genes in both brain areas, and to common prefrontal and striatal changes in myelin markers of functionality and stability. These findings were confirmed and extended by MRI and immunohistochemical results, while epigenetic analyses pointed to DNA methylation as the underlying mechanism responsible for these effects. Our present study thus provides novel and corroborating evidence towards the characterization of the long-lasting molecular signature of late prenatal infection in the mPFC and NAc of exposed offspring.

Our transcriptomic and epigenetic analyses regarding the effects of prenatal infection were conducted against the background of overt behavioural and cognitive phenotypes. Here, we confirmed the deleterious effects of prenatal poly(I:C) exposure on working memory and social interaction (Bitanihirwe BK, D Peleg-Raibstein, et al. 2010; Bitanihirwe BK, L Weber, et al. 2010; Richetto J et al. 2013), suggesting that prenatal viral-like immune activation leads to robust deficits in these cognitive and behavioural domains. Against the background of these impairments, we further identified transcriptomic, epigenetic, and neuroanatomical abnormalities in offspring exposed to prenatal immune activation. This approach thus allowed us to assess possible molecular correlates of the behavioural and cognitive abnormalities induced by prenatal immune challenge.

Our genome-wide gene expression analyses revealed transcriptomic alterations in a number of genes, many of which have been associated with schizophrenia. In particular, when comparing our results with the currently recognized risk genes for schizophrenia, 5 of the affected genes in the mPFC (ADORA2A, CNP, DRD2, MAG, PPP1RB1), and 21 of the affected genes in the NAc (APOD, CACNA 1B, DRD3, FOXP2, GLS, GRIN2A, HIST1H2BC, HRT1A, HRT2A, HRT4, MAG, MGST1, MYO16, OXT, PBRM1, PDYN, ST3GAL1, SULT4A1, TSNAX, VAMP4) fall into this list (Butler MG et al. 2015).

In agreement with previous reports by Connor et al. (2012) and Smith et al. (2007), prenatal immune activation leads to less extensive gene expression changes in the mPFC (n=116 genes) as compared to the NAc (n=251 genes) (Smith SE et al. 2007; Connor CM et al. 2012). Moreover, consistent with these earlier reports (Connor CM et al. 2012) most transcripts in prenatally infected offspring show less than 2-fold changes from the control group. Such effect sizes are not unprecedented given the early prenatal timing of the environmental insult, which typically leads to pathological changes in brain and behaviour that are widespread but often relatively mild in terms of effect size (Meyer U et al. 2007). Despite the magnitude and number of changes, these effects may still be pathophysiologically relevant and may prime the organism to altered neuronal functions when challenged with other environmental stressors or behavioural and cognitive demands.

Notably, some of our data are consistent with previous findings in the prenatal influenza infection model developed by Fatemi and colleagues, suggesting that at least parts of the transcriptomic changes induced by prenatal influenza exposure may be mediated indirectly via activation of the maternal immune system (Fatemi

SH et al. 2012). As in the prenatal influenza model, we observed changes in the expression of FOXP2, PPP1R1B, DEAD box polypeptide, ATP13, CRYGE, and various other genes implicated in the pathophysiology of schizophrenia and autism (Fatemi SH et al. 2005; Fatemi SH et al. 2008; Fatemi SH, TD Folsom, TJ Reutiman, D Abu-Odeh, et al. 2009; Fatemi SH, TD Folsom, TJ Reutiman, H Huang, et al. 2009). The similarities between the two models are even more evident when considering the region-overlapping transcriptomic effects identified here. Indeed, among the 14 genes commonly affected in the mPFC and in the NAc, 6 of these (MAG, MOG, MOBP, MAL, CLDN11 and MYRF) are similarly affected by prenatal exposure to influenza (Fatemi SH et al. 2005; Fatemi SH, TD Folsom, TJ Reutiman, D Abu-Odeh, et al. 2009) and are involved in myelin functionality and stability. The consistency between our findings and those reported by Fatemi and colleagues thus suggests that reduced expression of markers of myelin stability and functionality could be a long-lasting molecular signature of this prenatal immune activation. Additional support for this hypothesis also stems from recent proteomic analyses demonstrating similar effects of prenatal viral-like immune activation on myelination-related proteins (Farrelly L et al. 2015). Indeed, Farrelly et al. (2015) also uncovered changes in myelin related proteins, such as MBP1 and rhombex 29, suggesting that prenatal infection may contribute to increasing the risk for schizophrenia through mechanisms involving myelin formation and functionality (Farrelly L et al. 2015).

The effects of prenatal immune activation on myelin-related dysfunctions are particularly interesting in light of the potential role of myelination and white matter abnormalities present in schizophrenia and related disorders (Haroutunian V et al. 2014; Mighdoll MI et al. 2015; Chavarria-Siles I et al. 2016). Indeed, myelin

provides the basis for rapid impulse conduction in the central nervous system and acts as electrical insulation for the unsheathed axon, which both helps to preserve the amplitude and increase the conduction velocity of the propagating axonal potential (Nave KA and HB Werner 2014; Normand EA and MN Rasband 2015). Given these essential functions, it is not surprising that damage to the myelin structure has been implicated in a variety of neurodevelopmental disorders. The expression of MAG, MOG, MOBP, MAL and CLDN11 is physiologically enriched in myelin-forming oligodendrocytes and is down-regulated in schizophrenic subjects (Hakak Y et al. 2001; Aston C et al. 2004; Katsel P et al. 2005; Le-Niculescu H et al. 2009). Genetic association studies have further established a potential link between polymorphisms in oligodendrocyte-related genes and specific sub-populations of schizophrenia patients (Wan C et al. 2005; Yang YF et al. 2005; Zai G et al. 2005; Liu YH et al. 2013). Moreover, alterations in white matter, such as volume reductions in prefrontal areas and increased density in subcortical areas, morphologic abnormalities in oligodendroglia and myelin-related gene abnormalities have all been related to schizophrenia (Sanfilipo M, T Lafargue, L Arena, et al. 2000; Sanfilipo M, T Lafargue, H Rusinek, et al. 2000; Davis KL and V Haroutunian 2003; Davis KL et al. 2003; Connor CM et al. 2011). Our findings here, together with those reported by Fatemi et al. and Farrelly et al. (Fatemi SH et al. 2005; Fatemi SH, TD Folsom, TJ Reutiman, D Abu-Odeh, et al. 2009; Fatemi SH, TD Folsom, TJ Reutiman, H Huang, et al. 2009; Farrelly L et al. 2015), highlight that the pathological relationship between prenatal infection and neurodevelopmental psychiatric disorders involves the disruption of myelination-related processes.

We performed additional MRI and immunohistochemical investigations to examine whether abnormal expression of myelination-related genes may have an impact on grey and white matter structure. A single study has previously reported white and grey matter microstructural alterations detected using diffusion tensor imaging (DTI) in polyI:C exposed mice (Li Q et al. 2010). Importantly however, whilst alterations in myelin content may influence DTI and relaxation-time measurements, these do not represent either specific or quantitative measures of myelin content as they are influenced by other biophysical and biochemical processes that occur during brain maturation. These include neuronal ramification, synaptogenesis, changing protein composition of the extracellular matrix and alterations in membrane permeability. A robust alternative approach to estimating myelin content is Myelin Water Fraction (MWF) imaging (MacKay A et al. 1994). These methods, including mcDESPOT (Deoni SC et al. 2008; Deoni SC 2011; Deoni SC et al. 2013) as employed in the current study, aim to separate the measured MR signal into contributions from anatomically distinct water compartments, slow relaxing intra- and extra-axonal water and faster relaxing water trapped in-between myelin bilayers. Importantly, MWF measures have been shown to correlate strongly with “gold-standard” histological estimates of myelin content (Beaulieu C et al. 1998; Gareau PJ et al. 2000; Laule C et al. 2006; Laule C et al. 2008) and have been used to investigate neurodevelopment in infants (Deoni SC et al. 2011; Deoni SC et al. 2012).

The current study therefore represents the first application of mcDESPOT to a rodent model of neurodevelopmental disorders. Using unbiased brain-wide tensor based morphometry, we observed significant volumetric increases in cortical areas of polyI:C exposed offspring. Voxel-wise analysis of the mcDESPOT data revealed

significant decreases in T_2 relaxation time. The latter overlaps spatially with regions of volumetric expansion in the cortex, but also regions that contract (e.g. thalamus, cerebellum), and regions that show no apparent volumetric changes (e.g. amygdala, hippocampus), sub-cortically, arguing against a simple biophysical effect of shortened T_2 driving apparent anatomical changes in the images (Cousins DA et al. 2013). Mapping of C57Bl6 mouse brain maturation post-weaning using automated morphometry suggests that grey matter regions reach their final volume within the first eight postnatal weeks, with no further global or local volume changes observable after this point (Hammelrath L et al. 2016). In contrast, there is an initial decrease of T_2 both in white and in grey matter from three to eight weeks postnatal, after which T_2 values steadily increase up to at least 24 weeks of age (Hammelrath L et al. 2016). These changes are consistent with prior observations in both rats (Samorajski T and C Rolsten 1973) and humans with increasing post-gestational age (Huppi PS and J Dubois 2006). Our present observations of significantly increased cortical volume, coupled with decreased T_2 relaxation times in 12-week old GD17 polyI:C offspring in comparison to saline controls, strongly suggests these effects represent a developmental lag in the maturation of the brain in the polyI:C -exposed offspring. In support of this notion, we have recently shown that prenatal immune activation leads to an “immature” cortical GABAergic network in adulthood (Richetto J et al. 2014). In contrast to our data, longitudinal MRI-analyses of rats exposed to polyI:C on GD15, suggest that the volume of the prefrontal cortex, striatum and hippocampus are significantly reduced compared to saline controls at 12 weeks of age (Piontkewitz Y et al. 2011). However, this discrepancy likely reflects the different maturational profile of the mouse and rat brains (Mengler L et al. 2014; Hammelrath L et al. 2016).

Indeed, rat cortical and striatal grey matter volume reaches a plateau at 8-9 weeks of age. The smaller cortical and striatal volumes in POL-exposed rats is therefore perhaps also consistent with a delayed maturational profile (Piontkewitz Y et al. 2011).

In contrast to the changes in T_2, we found no significant alterations in either T_1 or the MWF. Based on these data, we therefore hypothesise that the T_2 decrease emerging in immune-challenged offspring may not represent a deficit in myelination *per se*, but rather, could be the result of micro-structural alterations in myelin and myelin sheaths which may affect their stability or function. Although this hypothesis warrants further investigation, it is consistent with the known roles of MAG, MOBP, MAL and MOG in the stabilization, function and structure of oligodendrocytes and the myelin sheath (Frank M 2000; Montague P et al. 2006; Quarles RH 2007; Schnaar RL and PH Lopez 2009). Furthermore, we observed no changes in myelin basic protein (MBP) content in the prefrontal cortex, both in terms of gene expression and immunohistochemistry. These data are also consistent with the lack of significant changes in the MWF signal. MBP is one of the two principal protein components of myelin (Wong JH et al. 2014) and is often taken as an indicator of myelin state and content (Vassall KA et al. 2015; Hashimoto M et al. 2016), suggesting that it might not be the 'quantity' of myelin *per se* that is affected by the prenatal manipulation, but rather the 'quality'. Our observation of a decrease in MOBP protein levels in the PFC of polyI:C exposed offspring may be consistent with this notion. Although speculative, such deficits in myelin stability may potentially underpin reported observations of disrupted long-range neural synchrony in polyI:C exposed rodents (Dickerson DD et al. 2010).

Further studies investigating brain function at the macroscale and myelin sheaths at the ultra-structural (EM) level are clearly required.

Lastly, our study provides the first report concerning hyper-methylation of the MOBP promoter following prenatal infection. Hence, we identify an epigenetic mechanism that could translate the effects of prenatal infection into long-lasting transcriptomic changes in myelination-related genes. Epigenetic modifications may, indeed, represent an important factor contributing to the disruption of brain development and behavioral functions in response to exposure to prenatal adversities such as infection (Bale TL 2015; Bohacek J and IM Mansuy 2015). Epigenetic changes such as DNA hyper- or hypomethylation, histone modifications, and altered micro-RNA expression have already been identified in models of prenatal immune activation (Connor CM et al. 2012; Tang B et al. 2013; Basil P et al. 2014; Labouesse MA et al. 2015). As DNA hyper-methylation often leads to the formation of transcriptionally inactive chromatin, which in turn readily impedes gene transcription mechanisms (Bale TL 2015; Bohacek J and IM Mansuy 2015; Szyf M 2015), hyper-methylation of the MOBP promoter could be the causative mechanism responsible of the reduced gene and protein expression levels observed after late prenatal immune activation. Future studies are warranted to examine whether these epigenetic changes are present in multiple brain regions other than the prefrontal cortex.

In conclusion, our study further characterizes the molecular signature of prenatal viral-like infection in the brains of exposed offspring. In particular, prenatal infection-induced transcriptomic changes in myelination-related genes seems to be a common pathological feature in multiple brain areas and may be, at least in part, mediated by persistent effects on DNA hypermethylation. The current study

also provides the first voxel-wise assessment of brain volume and application of MCR methodology, which together suggest a putative delay in brain maturation following prenatal viral-like infection, in the absence of demyelination *per se*. However, the mechanistic links between these molecular modifications and MR-detectable brain alterations occurring in prenatally infected offspring remains unclear and warrants future investigations.

Table 1

Gene	Fold change	p-value
Adamts4	-1.259	0.00291
Adora2a	-1.260	0.02701
Adra2a	-1.222	0.01440
Bcas1	-1.242	0.00095
Cabp7	-1.232	0.03128
Cdca7	-1.225	0.00062
Cldn11	-1.356	0.00088
Clic4	-1.216	0.00030
Cnp	-1.265	0.00317
Cpm	-1.215	0.00897
Cryge	-1.657	0.04590
Cyp2j12	-1.215	0.00246
Cyp4a28-ps	-1.330	0.00077
Dlk1	-1.215	0.03507
Dnali1	-1.205	0.00218
Drd2	-1.453	0.03478
Fa2h	-1.297	0.01749
Galnt6	-1.259	0.00046
Gas5	-1.721	0.00002
Glp1r	-1.360	0.02303
Gpr6	-1.405	0.01594
Gstm6	-1.241	0.01346
Hist1h2bb	-1.269	0.00025
Hist1h2bq	-1.202	0.00064
Lrrc10b	-1.273	0.00186
Mag	-1.261	0.01173
Mal	-1.312	0.00395
Mobp	-1.417	0.00124
Mog	-1.250	0.02082
mt-Ta	-3.146	0.00019
mt-Tq	-1.253	0.02654
mt-Tv	-1.322	0.01354
Myrf	-1.229	0.00307
Nnat	-1.266	0.00510
Nxph3	-1.211	0.02714
Opalin	-1.333	0.02207
Pcp4l1	-1.204	0.02124
Ppp1r1b	-1.205	0.00369
Prelp	-1.209	0.01465
Rem2	-1.203	0.00109
Rny1	-1.558	0.00612
Rpl7a	-1.207	0.00078
Rps27rt	-1.206	0.00008
Rybp	-1.205	0.00002
Sf3b4	-1.234	0.01561
Shisa6	-1.216	0.00798
Sox4	-1.231	0.00129
Thbs4	-1.455	0.00133
Trf	-1.235	0.00786
Tspan2	-1.236	0.00875
Txnip	-1.210	0.04400
Ube2v1	-1.237	0.00744
Ugt8a	-1.203	0.02783
Zcchc12	-1.213	0.01511
Zic1	-1.301	0.03720

Table 1. The table represents the 55 downregulated genes in the mPFC as revealed by microarray. All data are based on *N*(CON) = 6, *N*(POL) = 6.

Table 2

Gene	Fold change	p-value
Aak1	1.212	0.00227
Adamts10	1.217	0.00008
Atp11b	1.300	0.00070
BC005561	1.221	0.00146
BC030499	1.493	0.00080
Cdh12	1.218	0.00004
Chuk	1.202	0.00032
Coro6	1.318	0.00003
Cpne9	1.223	0.00090
Cspp1	1.234	0.00005
Ddx26b	1.267	0.00126
Dnajc13	1.212	0.00141
Echdc2	1.238	0.01081
Eif2s3y	1.446	0.02942
Eml5	1.234	0.00236
Fam178a	1.236	0.00081
Fat3	1.276	0.00084
Fcf1	1.209	0.00307
Firre	1.204	0.04499
Flnb	1.221	0.00683
Gpatch8	1.287	0.00472
Gtf3c2	1.209	0.01987
Herc6	1.244	0.00051
Hnrnpu	1.463	0.00304
Kansl1	1.348	0.01338
Leng8	1.372	0.00557
Luc7l3	1.220	0.00244
Malat1	1.343	0.01141
Meg3	1.312	0.00568
Mirg	1.398	0.00012
mt-Ty	1.251	0.00880
Myo9a	1.244	0.00058
Npas4	1.587	0.01846
Nup93	1.239	0.00071
Nvl	1.246	0.00027
Paxbp1	1.225	0.00141
Phf20l1	1.232	0.01339
Pisd-ps1	1.240	0.02393
Pisd-ps2	1.206	0.00064
Pnet-ps	1.290	0.01531
Pnisr	1.332	0.00103
Prpf39	1.299	0.00094
Rbm12b2	1.238	0.00561
Rbm33	1.318	0.00284
Rnpc3	1.321	0.00096
Rps6kb2	1.225	0.00088
Rxfp1	1.211	0.00002
Sfswap	1.218	0.00018
Slc9b2	1.221	0.00003
Smpd4	1.262	0.00036
Snhg11	1.269	0.00258
Taf1d	1.228	0.00118
Tfrc	1.205	0.00033
Tmem181a	1.246	0.00040
Trank1	1.340	0.00047
Ttc14	1.364	0.00064
Uggt2	1.381	0.00061
Vmn2r84	1.307	0.00099
Vmn2r86	1.578	0.00221
Wsb1	1.243	0.00812

Zcchc7	1.235	0.00203

Table 2. The table lists the 61 upregulated genes in the mPFC as revealed by microarray. All data are based on *N*(CON) = 6, *N*(POL) = 6.

Table 3

Gene	Fold change	p-value
Agt	-1.733	0.0412
Ankub1	-1.333	0.0261
Anln	-1.293	0.0299
Apod	-1.226	0.0014
Arhgdib	-1.300	0.0182
Arsg	-1.248	0.0006
Aspa	-1.352	0.0117
Atp13a4	-1.210	0.0284
BC005624	-1.204	0.0000
Bcas1	-1.250	0.0009
Cacng4	-1.226	0.0154
Calml4	-1.267	0.0372
Capsl	-1.353	0.0452
Ccdc170	-1.222	0.0401
Cd63	-1.298	0.0066
Cd82	-1.343	0.0055
Cdhr3	-1.379	0.0424
Chd6	-1.207	0.0247
Chd7	-1.215	0.0308
Cldn10	-1.213	0.0073
Cldn11	-1.227	0.0028
Clmn	-1.243	0.0309
Cobl	-1.216	0.0254
Coch	-1.378	0.0081
Crabp1	-1.296	0.0034
Cspp1	-1.255	0.0247
Ctnna1	-1.221	0.0016
Cyp2j9	-1.270	0.0019
Dnah3	-1.358	0.0258
Ebf1	-1.330	0.0005
Ebf2	-1.267	0.0446
Ebf3	-1.321	0.0181
Edil3	-1.210	0.0134
Eif3e	-1.250	0.0011
Elovl7	-1.343	0.0338
Enpp2	-1.691	0.0318
Ephx1	-1.209	0.0028
Evi2a	-1.246	0.0064
Fmo1	-1.219	0.0106
Frem3	-1.213	0.0017
Gab1	-1.210	0.0021
Gal	-2.353	0.0002
Galr1	-1.307	0.0126
Glis3	-1.255	0.0121
Gpr37	-1.293	0.0084
Gstm6	-1.225	0.0242
Hist1h1c	-1.409	0.0002
Hist1h2bc	-1.265	0.0036
Hmcn1	-1.236	0.0018
Iqcg	-1.300	0.0422
Iqcj	-1.209	0.0017
Itpkb	-1.270	0.0449
Kif6	-1.206	0.0040
Mag	-1.241	0.0223
Mal	-1.318	0.0013
Meig1	-1.416	0.0274
Mgst1	-1.266	0.0023
Mobp	-1.423	0.0000
Mog	-1.263	0.0121
Mpeg1	-1.293	0.0007
mt-Tf	-1.233	0.0018
mt-Tn	-1.591	0.0033
Mtx2	-1.209	0.0123
Myrf	-1.313	0.0009

Ndrg1	-1.237	0.0083
Nhp2	-1.331	0.0112
Nme5	-1.241	0.0096
Nr2f2	-1.698	0.0014
Nsmce4a	-1.232	0.0010
Opalin	-1.480	0.0015
Oxt	-1.322	0.0018
Pcolce2	-1.338	0.0081
Pde8a	-1.223	0.0056
Phldb1	-1.247	0.0013
Pigk	-1.203	0.0018
Pir	-1.218	0.0032
Pld1	-1.210	0.0284
Pllp	-1.301	0.0011
Prlr	-2.081	0.0194
Prox1	-1.400	0.0171
Prr18	-1.224	0.0049
Prrg4	-1.267	0.0325
Psma1	-1.200	0.0039
Rarres2	-1.234	0.0476
Rassf2	-1.270	0.0008
Rdm1	-1.675	0.0130
Rgs10	-1.238	0.0101
Rgs3	-1.292	0.0011
Ror1	-1.233	0.0250
Rpl26	-1.264	0.0036
Rpl35a	-1.212	0.0126
Rpl36	-1.203	0.0054
S1pr5	-1.252	0.0037
Scarna13	-1.446	0.0097
Sccpdh	-1.275	0.0102
Sgms2	-1.253	0.0221
Shank2	-1.478	0.0088
Slirp	-1.269	0.0115
Smco3	-1.234	0.0137
Sorcs1	-1.228	0.0014
Sparc	-1.289	0.0360
Spef2	-1.474	0.0195
St6galnac1	-1.222	0.0006
Stxbp3a	-1.258	0.0001
Synpo2	-1.308	0.0016
Tac2	-2.333	0.0005
Tcf7l2	-1.341	0.0309
Tcn2	-1.223	0.0208
Tm4sf1	-1.225	0.0454
Tmbim1	-1.235	0.0033
Tmem212	-1.250	0.0335
Tmem215	-1.215	0.0010
Tnfaip6	-1.236	0.0133
Trdn	-1.242	0.0017
Trh	-1.303	0.0038
Ttc21a	-1.221	0.0254
Ttr	-7.075	0.0118
Unc13c	-1.275	0.0141
Vamp4	-1.315	0.0003
Vps4b	-1.219	0.0005
Wdr49	-1.286	0.0091
Wdr63	-1.205	0.0120
Wdr96	-1.228	0.0156
Whrn	-1.278	0.0360
Zbtb10	-1.209	0.0080
Zfhx3	-1.217	0.0384

Table 3. The table lists the 126 downregulated genes in the NAc as revealed by microarray. All data are based on *N*(CON) = 6, *N*(POL) = 6.

Table 4

Gene	Fold change	p-value
Adamts3	0.0018	1.325
Adat3	0.0168	1.235
Adh5	0.0049	1.202
Ahr	0.0005	1.234
Ankrd45	0.0001	1.275
Apbb3	0.0003	1.215
Arpc5	0.0437	1.206
Azin1	0.0002	1.288
B3galt2	0.0164	1.443
Bcl11a	0.0393	1.203
Bmp3	0.0488	1.292
Brinp2	0.0127	1.225
Btbd3	0.0163	1.238
Cabp7	0.0108	1.270
Cacna2d1	0.0091	1.325
Cacnb3	0.0270	1.210
Cckbr	0.0399	1.371
Cecr6	0.0433	1.226
Clec2l	0.0088	1.226
Cnih3	0.0174	1.455
Cntnap3	0.0394	1.270
Col6a1	0.0023	1.329
Crebbp	0.0001	1.201
Csgalnact1	0.0034	1.325
Ctgf	0.0466	1.664
Dab1	0.0143	1.221
Dclk3	0.0219	1.218
Dkk3	0.0188	1.216
Drd3	0.0005	1.507
Dsg1a	0.0003	1.277
Dsg1c	0.0012	1.242
Echdc2	0.0246	1.200
Eri2	0.0148	1.293
Fam131a	0.0041	1.388
Fgf10	0.0139	1.230
Foxp2	0.0144	1.215
Galnt9	0.0261	1.326
Gls	0.0120	1.287
Gnrh1	0.0243	1.272
Gpr126	0.0066	1.277
Gpr149	0.0203	1.284
Gpr26	0.0138	1.355
Grin2a	0.0381	1.262
Gtpbp2	0.0003	1.204
Gtpbp8	0.0397	1.322
Hmgcr	0.0216	1.215
Hsd17b7	0.0254	1.262
Hspbp1	0.0250	1.233
Htr1a	0.0264	1.387
Htr2a	0.0410	1.360
Htr4	0.0019	1.316
Igsf21	0.0290	1.322
Islr2	0.0137	1.319
Itpka	0.0086	1.231
Kcnab3	0.0096	1.251
Kcnh3	0.0390	1.232
Kctd16	0.0410	1.247
Kifc2	0.0029	1.231
Lix1	0.0084	1.270
Lmo4	0.0011	1.201
Lrrc55	0.0065	1.318
Mafg	0.0026	1.205
Mef2c	0.0214	1.304
Mef2d	0.0040	1.287
Mgll	0.0019	1.267
Morn4	0.0087	1.201
Mpped1	0.0295	1.331
Myo16	0.0017	1.345
Napb	0.0460	1.232
Ndnf	0.0403	1.341
Ndufa13	0.0015	1.201
Nmbr	0.0373	1.776

Nov	0.0160	2.691
Npas4	0.0214	1.574
Nptx1	0.0140	1.645
Npy1r	0.0316	1.303
Ntn1	0.0062	1.291
Nxph3	0.0295	1.302
Ociad2	0.0208	1.265
Olfm3	0.0229	1.248
Pbrm1	0.0279	1.228
Pcsk5	0.0020	1.229
Pdcd4	0.0236	1.213
Pde1a	0.0028	1.341
Pdyn	0.0358	1.251
Pls3	0.0446	1.211
Pou3f4	0.0369	1.201
Ppp1r12b	0.0074	1.234
Prr14l	0.0214	1.238
Rap1gap2	0.0301	1.207
Rapgefl1	0.0103	1.337
Rasl10b	0.0222	1.215
Rfk	0.0258	1.237
Rnf26	0.0257	1.217
Rnf39	0.0059	1.267
Satb1	0.0366	1.274
Sema5b	0.0107	1.235
Sidt1	0.0278	1.432
Slc17a7	0.0490	2.840
Slc2a3	0.0018	1.242
Slc7a4	0.0016	1.224
Slco5a1	0.0030	1.234
Slit2	0.0420	1.279
Sprn	0.0206	1.263
Spryd3	0.0266	1.205
St3gal1	0.0005	1.619
Stard5	0.0063	1.685
Stra6	0.0103	1.396
Strip2	0.0427	1.239
Sult4a1	0.0106	1.299
Svop	0.0070	1.232
Szt2	0.0013	1.283
Tenm4	0.0027	1.233
Tmem132d	0.0456	1.205
Tmem160	0.0015	1.317
Tmem56	0.0439	1.206
Tpbg	0.0085	1.215
Trim23	0.0175	1.254
Tsnax	0.0001	1.245
Ttc39b	0.0325	1.234
Ube3b	0.0018	1.224
Uck2	0.0160	1.220
Uqcrc1	0.0000	1.251
Wdr54	0.0008	1.258
Wnt2	0.0051	1.286

Table 4. The table lists the 125 upregulated genes in the NAc as revealed by microarray. All data are based on *N*(CON) = 6, *N*(POL) = 6.

Legends

Figure 1. Cognitive and behavioral deficits following late prenatal immune activation. Mice were subjected to prenatal poly(I:C) treatment on gestation day 17 (POL), or they were exposed to prenatal control (CON) treatment. **(A)** Percent time spent in the novel arm during the Y-maze working memory test. *p < 0.05 based on independent Student's t tests (two-tailed). **(B)** Percent time spent with an unfamiliar live mouse, relative to an inanimate dummy object, during the social interaction test, and percent time spent with a novel live mouse, relative to a familiar one, during the social recognition test. *p < 0.05 and ***p < 0.001 based on independent Student's t tests (two-tailed). All data are based on N(CON) = 10, N(POL) = 10.

Figure 2. Unique and common gene expression differences following late prenatal immune activation in the mPFC and NAc, revealed by microarry. Mice were subjected to prenatal poly(I:C) treatment on gestation day 17 (POL), or they were exposed to prenatal control (CON) treatment. **(A)** Hierarchical clustering of differentially expressed genes in POL offspring relative to CON offspring in the mPFC and NAc. Down- and up-regulated genes are represented in purple and yellow color, respectively. **(B)** Venn Diagram depicting the number of genes that are uniquely and commonly affected in the mPFC and NAc of POL offspring. The commonly affected genes are listed, and down- and up-regulated genes are represented by blue and red color, respectively, in each brain area. All data are based on N(CON) = 6, N(POL) = 6.

Figure 3. Validation of common myelin gene expression differences in the mPFC and NAc. Mice were subjected to prenatal poly(I:C) treatment on gestation day 17 (POL), or they were exposed to prenatal control (CON) treatment .**(A)** The bar plots represent the mRNA levels of each selected gene (% *versus* CON). The gene expression levels were assessed by RT-qPCR. *p < 0.05, **p < 0.01 and ***p < 0.001 based on independent Student's t tests (two-tailed). All data are based on N(CON) = 10, N(POL) = 10. **(B)** Graphical representation of the network analysis conducted on the commonly affected myelin genes. The analysis was conducted using Ingenuity Pathway Analysis (IPA), and each gene is represented in relation to the others and to the specific functions it is involved in. **1** = Ensheathment of axons; **2** = Myelination; **3** = Myelination of cells; **4** = Myelination of nerves; **5** = Dendritic growth and branching.

Figure 4. Alterations in neuroanatomy following late prenatal infection revealed by brain-wide tensor based morphometry analysis of 3D T_2-weighted MR images. Mice were subjected to prenatal poly(I:C) treatment on gestation day 17 (POL), or they were exposed to prenatal control (CON) treatment. Data shown are raw values for log jacobian determinant and effect (t-statistic) thresholded at p<0.01 uncorrected and false discovery rate corrected at q<0.05.

Figure 5. Alterations in T_1, T_2 relaxation time and myelin water fraction (MWF) following late prenatal infection as revealed by voxel-wise cluster analysis. Mice were subjected to prenatal poly(I:C) treatment on gestation day 17 (POL), or they were exposed to prenatal control (CON) treatment. Data shown for each parameter are the raw effects "t" (t-statistic) and significant voxel-wise changes in each tissue parameter relative to the control group thresholded at q<0.05 (False discovery rate corrected).

Figure 6. Protein expression alterations following late prenatal infection, as revealed by immunohistochemistry. Mice were subjected to prenatal poly(I:C) treatment on gestation day 17 (POL), or they were exposed to prenatal control (CON) treatment. **(A)** The bar plots represent the percent area of immunoreactive pixels for MBP. **(B)** The bar plots represent the percent area of immunoreactive pixels for MOBP. Representative photomicrographs of MBP and MOBP are presented in figure 6a and 6b, respectively at

x4 magnifications, scale bar = 50 µm. ACC, anterior cingulate cortex; PrL, prelimbic cortex; Irl, infralimbic cortex. For MBP: *N*(CON) = 10, *N*(POL-) = 9; *p*=0.426, Cohens'd=0.088, Student's T-Test (one tailed). For MOBP: *N*(CON) = 7, *N*(POL) = 8; *p*=0.041, Cohens'd=0.961, Student's T-Test (one tailed).

Figure 7. Investigation of DNA methylation differences in the promoter of the MOBP gene using EpiTYPER. Mice were subjected to prenatal poly(I:C) treatment on gestation day 17 (POL), or they were exposed to prenatal control (CON) treatment. **(A)** Graphical representation of the MOBP gene and genomic locations of the selected amplicons. **(B)** Sequences of the selected amplicons and position of investigated CpGs in each amplicon. Methylation of the numbered CpGs (in bold font) was accessible to quantification by EpiTYPER, whereas underlined CpGs were un-measurable for technical reasons. **(C)** Percent DNA methylation of specific CpGs in the selected amplicons. **p* < 0.05, ***p* < 0.01, and ****p* < 0.001, reflecting the significant differences between CON and POL offspring; based on post-hoc tests following the presence of a significant interaction between prenatal treatment and position in ANOVA (Amplicon 1: $(F_{(6,54)} = 5.35, p < 0.001$ Amplicon 2: $F_{(1,9)} = 7.32, p < 0.05$). *N*(CON) = 6, *N*(POL-) = 5,

References

Aston C, Jiang L, Sokolov BP. 2004. Microarray analysis of postmortem temporal cortex from patients with schizophrenia. J Neurosci Res 77:858-866.
Bale TL. 2015. Epigenetic and transgenerational reprogramming of brain development. Nat Rev Neurosci 16:332-344.
Basil P, Li Q, Dempster EL, Mill J, Sham PC, Wong CC, McAlonan GM. 2014. Prenatal maternal immune activation causes epigenetic differences in adolescent mouse brain. Transl Psychiatry 4:e434.
Beaulieu C, Fenrich FR, Allen PS. 1998. Multicomponent water proton transverse relaxation and T2-discriminated water diffusion in myelinated and nonmyelinated nerve. Magn Reson Imaging 16:1201-1210.
Bitanihirwe BK, Peleg-Raibstein D, Mouttet F, Feldon J, Meyer U. 2010. Late prenatal immune activation in mice leads to behavioral and neurochemical abnormalities relevant to the negative symptoms of schizophrenia. Neuropsychopharmacology 35:2462-2478.
Bitanihirwe BK, Weber L, Feldon J, Meyer U. 2010. Cognitive impairment following prenatal immune challenge in mice correlates with prefrontal cortical AKT1 deficiency. Int J Neuropsychopharmacol 13:981-996.
Bohacek J, Mansuy IM. 2015. Molecular insights into transgenerational non-genetic inheritance of acquired behaviours. Nat Rev Genet 16:641-652.
Brown AS. 2011. The environment and susceptibility to schizophrenia. Prog Neurobiol 93:23-58.
Brown AS, Derkits EJ. 2010. Prenatal infection and schizophrenia: a review of epidemiologic and translational studies. Am J Psychiatry 167:261-280.
Butler MG, McGuire AB, Masoud H, Manzardo AM. 2015. Currently recognized genes for schizophrenia: High-resolution chromosome ideogram representation. Am J Med Genet B Neuropsychiatr Genet.
Chavarria-Siles I, White T, de Leeuw C, Goudriaan A, Lips E, Ehrlich S, Turner JA, Calhoun VD, Gollub RL, Magnotta VA, Ho BC, Smit AB, Verheijen MH, Posthuma D. 2016. Myelination-related genes are associated with decreased white matter integrity in schizophrenia. Eur J Hum Genet 24:381-386.
Clancy B, Kersh B, Hyde J, Darlington RB, Anand KJ, Finlay BL. 2007. Web-based method for translating neurodevelopment from laboratory species to humans. Neuroinformatics 5:79-94.
Connor CM, Crawford BC, Akbarian S. 2011. White matter neuron alterations in schizophrenia and related disorders. Int J Dev Neurosci 29:325-334.
Connor CM, Dincer A, Straubhaar J, Galler JR, Houston IB, Akbarian S. 2012. Maternal immune activation alters behavior in adult offspring, with subtle changes in the cortical transcriptome and epigenome. Schizophr Res 140:175-184.
Cousins DA, Aribisala B, Nicol Ferrier I, Blamire AM. 2013. Lithium, gray matter, and magnetic resonance imaging signal. Biol Psychiatry 73:652-657.
Davis KL, Haroutunian V. 2003. Global expression-profiling studies and oligodendrocyte dysfunction in schizophrenia and bipolar disorder. Lancet 362:758.
Davis KL, Stewart DG, Friedman JI, Buchsbaum M, Harvey PD, Hof PR, Buxbaum J, Haroutunian V. 2003. White matter changes in schizophrenia: evidence for myelin-related dysfunction. Arch Gen Psychiatry 60:443-456.
Deoni SC. 2011. Magnetic resonance relaxation and quantitative measurement in the brain. Methods Mol Biol 711:65-108.
Deoni SC, Dean DC, 3rd, O'Muircheartaigh J, Dirks H, Jerskey BA. 2012. Investigating white matter development in infancy and early childhood using myelin water faction and relaxation time mapping. Neuroimage 63:1038-1053.
Deoni SC, Matthews L, Kolind SH. 2013. One component? Two components? Three? The effect of including a nonexchanging "free" water component in multicomponent driven equilibrium single pulse observation of T1 and T2. Magn Reson Med 70:147-154.

Deoni SC, Mercure E, Blasi A, Gasston D, Thomson A, Johnson M, Williams SC, Murphy DG. 2011. Mapping infant brain myelination with magnetic resonance imaging. J Neurosci 31:784-791.
Deoni SC, Williams SC, Jezzard P, Suckling J, Murphy DG, Jones DK. 2008. Standardized structural magnetic resonance imaging in multicentre studies using quantitative T1 and T2 imaging at 1.5 T. Neuroimage 40:662-671.
Dickerson DD, Wolff AR, Bilkey DK. 2010. Abnormal long-range neural synchrony in a maternal immune activation animal model of schizophrenia. J Neurosci 30:12424-12431.
Eyles D, Feldon J, Meyer U. 2012. Schizophrenia: do all roads lead to dopamine or is this where they start? Evidence from two epidemiologically informed developmental rodent models. Transl Psychiatry 2:e81.
Farrelly L, Focking M, Piontkewitz Y, Dicker P, English J, Wynne K, Cannon M, Cagney G, Cotter DR. 2015. Maternal immune activation induces changes in myelin and metabolic proteins, some of which can be prevented with risperidone in adolescence. Dev Neurosci 37:43-55.
Fatemi SH, Folsom TD, Reutiman TJ, Abu-Odeh D, Mori S, Huang H, Oishi K. 2009. Abnormal expression of myelination genes and alterations in white matter fractional anisotropy following prenatal viral influenza infection at E16 in mice. Schizophr Res 112:46-53.
Fatemi SH, Folsom TD, Reutiman TJ, Huang H, Oishi K, Mori S. 2009. Prenatal viral infection of mice at E16 causes changes in gene expression in hippocampi of the offspring. Eur Neuropsychopharmacol 19:648-653.
Fatemi SH, Folsom TD, Rooney RJ, Mori S, Kornfield TE, Reutiman TJ, Kneeland RE, Liesch SB, Hua K, Hsu J, Patel DH. 2012. The viral theory of schizophrenia revisited: abnormal placental gene expression and structural changes with lack of evidence for H1N1 viral presence in placentae of infected mice or brains of exposed offspring. Neuropharmacology 62:1290-1298.
Fatemi SH, Pearce DA, Brooks AI, Sidwell RW. 2005. Prenatal viral infection in mouse causes differential expression of genes in brains of mouse progeny: a potential animal model for schizophrenia and autism. Synapse 57:91-99.
Fatemi SH, Reutiman TJ, Folsom TD, Huang H, Oishi K, Mori S, Smee DF, Pearce DA, Winter C, Sohr R, Juckel G. 2008. Maternal infection leads to abnormal gene regulation and brain atrophy in mouse offspring: implications for genesis of neurodevelopmental disorders. Schizophr Res 99:56-70.
Frank M. 2000. MAL, a proteolipid in glycosphingolipid enriched domains: functional implications in myelin and beyond. Prog Neurobiol 60:531-544.
Gareau PJ, Rutt BK, Karlik SJ, Mitchell JR. 2000. Magnetization transfer and multicomponent T2 relaxation measurements with histopathologic correlation in an experimental model of MS. J Magn Reson Imaging 11:586-595.
Genovese CR, Lazar NA, Nichols T. 2002. Thresholding of statistical maps in functional neuroimaging using the false discovery rate. Neuroimage 15:870-878.
Giovanoli S, Engler H, Engler A, Richetto J, Voget M, Willi R, Winter C, Riva MA, Mortensen PB, Feldon J, Schedlowski M, Meyer U. 2013. Stress in puberty unmasks latent neuropathological consequences of prenatal immune activation in mice. Science 339:1095-1099.
Hakak Y, Walker JR, Li C, Wong WH, Davis KL, Buxbaum JD, Haroutunian V, Fienberg AA. 2001. Genome-wide expression analysis reveals dysregulation of myelination-related genes in chronic schizophrenia. Proc Natl Acad Sci U S A 98:4746-4751.
Hammelrath L, Skokic S, Khmelinskii A, Hess A, van der Knaap N, Staring M, Lelieveldt BP, Wiedermann D, Hoehn M. 2016. Morphological maturation of the mouse brain: An in vivo MRI and histology investigation. Neuroimage 125:144-152.
Haroutunian V, Katsel P, Roussos P, Davis KL, Altshuler LL, Bartzokis G. 2014. Myelination, oligodendrocytes, and serious mental illness. Glia 62:1856-1877.

Harvey L, Boksa P. 2012. A stereological comparison of GAD67 and reelin expression in the hippocampal stratum oriens of offspring from two mouse models of maternal inflammation during pregnancy. Neuropharmacology 62:1767-1776.
Hashimoto M, Murata K, Ishida J, Kanou A, Kasuya Y, Fukamizu A. 2016. Severe Hypomyelination and Developmental Defects Are Caused in Mice Lacking Protein Arginine Methyltransferase 1 (PRMT1) in the Central Nervous System. J Biol Chem 291:2237-2245.
Horvath S, Mirnics K. 2015. Schizophrenia as a disorder of molecular pathways. Biol Psychiatry 77:22-28.
Huppi PS, Dubois J. 2006. Diffusion tensor imaging of brain development. Semin Fetal Neonatal Med 11:489-497.
Ibi D, Yamada K. 2015. Therapeutic Targets for Neurodevelopmental Disorders Emerging from Animal Models with Perinatal Immune Activation. Int J Mol Sci 16:28218-28229.
Katsel P, Davis KL, Haroutunian V. 2005. Variations in myelin and oligodendrocyte-related gene expression across multiple brain regions in schizophrenia: a gene ontology study. Schizophr Res 79:157-173.
Labouesse MA, Dong E, Grayson DR, Guidotti A, Meyer U. 2015. Maternal immune activation induces GAD1 and GAD2 promoter remodeling in the offspring prefrontal cortex. Epigenetics 10:1143-1155.
Laule C, Kozlowski P, Leung E, Li DK, Mackay AL, Moore GR. 2008. Myelin water imaging of multiple sclerosis at 7 T: correlations with histopathology. Neuroimage 40:1575-1580.
Laule C, Leung E, Lis DK, Traboulsee AL, Paty DW, MacKay AL, Moore GR. 2006. Myelin water imaging in multiple sclerosis: quantitative correlations with histopathology. Mult Scler 12:747-753.
Le-Niculescu H, Patel SD, Bhat M, Kuczenski R, Faraone SV, Tsuang MT, McMahon FJ, Schork NJ, Nurnberger JI, Jr., Niculescu AB, 3rd. 2009. Convergent functional genomics of genome-wide association data for bipolar disorder: comprehensive identification of candidate genes, pathways and mechanisms. Am J Med Genet B Neuropsychiatr Genet 150B:155-181.
Li Q, Cheung C, Wei R, Cheung V, Hui ES, You Y, Wong P, Chua SE, McAlonan GM, Wu EX. 2010. Voxel-based analysis of postnatal white matter microstructure in mice exposed to immune challenge in early or late pregnancy. Neuroimage 52:1-8.
Liu YH, Lai WS, Tsay HJ, Wang TW, Yu JY. 2013. Effects of maternal immune activation on adult neurogenesis in the subventricular zone-olfactory bulb pathway and olfactory discrimination. Schizophr Res 151:1-11.
MacKay A, Whittall K, Adler J, Li D, Paty D, Graeb D. 1994. In vivo visualization of myelin water in brain by magnetic resonance. Magn Reson Med 31:673-677.
Marangoni C, Hernandez M, Faedda GL. 2016. The role of environmental exposures as risk factors for bipolar disorder: A systematic review of longitudinal studies. J Affect Disord 193:165-174.
Mengler L, Khmelinskii A, Diedenhofen M, Po C, Staring M, Lelieveldt BP, Hoehn M. 2014. Brain maturation of the adolescent rat cortex and striatum: changes in volume and myelination. Neuroimage 84:35-44.
Meyer U. 2014. Prenatal poly(i:C) exposure and other developmental immune activation models in rodent systems. Biol Psychiatry 75:307-315.
Meyer U, Feldon J. 2010. Epidemiology-driven neurodevelopmental animal models of schizophrenia. Prog Neurobiol 90:285-326.
Meyer U, Feldon J, Fatemi SH. 2009. In-vivo rodent models for the experimental investigation of prenatal immune activation effects in neurodevelopmental brain disorders. Neurosci Biobehav Rev 33:1061-1079.
Meyer U, Feldon J, Schedlowski M, Yee BK. 2005. Towards an immuno-precipitated neurodevelopmental animal model of schizophrenia. Neurosci Biobehav Rev 29:913-947.

Meyer U, Nyffeler M, Engler A, Urwyler A, Schedlowski M, Knuesel I, Yee BK, Feldon J. 2006. The time of prenatal immune challenge determines the specificity of inflammation-mediated brain and behavioral pathology. J Neurosci 26:4752-4762.
Meyer U, Nyffeler M, Yee BK, Knuesel I, Feldon J. 2008. Adult brain and behavioral pathological markers of prenatal immune challenge during early/middle and late fetal development in mice. Brain Behav Immun 22:469-486.
Meyer U, Yee BK, Feldon J. 2007. The neurodevelopmental impact of prenatal infections at different times of pregnancy: the earlier the worse? Neuroscientist 13:241-256.
Mighdoll MI, Tao R, Kleinman JE, Hyde TM. 2015. Myelin, myelin-related disorders, and psychosis. Schizophr Res 161:85-93.
Montague P, McCallion AS, Davies RW, Griffiths IR. 2006. Myelin-associated oligodendrocytic basic protein: a family of abundant CNS myelin proteins in search of a function. Dev Neurosci 28:479-487.
Nave KA, Werner HB. 2014. Myelination of the nervous system: mechanisms and functions. Annu Rev Cell Dev Biol 30:503-533.
Normand EA, Rasband MN. 2015. Subcellular patterning: axonal domains with specialized structure and function. Dev Cell 32:459-468.
Oskvig DB, Elkahloun AG, Johnson KR, Phillips TM, Herkenham M. 2012. Maternal immune activation by LPS selectively alters specific gene expression profiles of interneuron migration and oxidative stress in the fetus without triggering a fetal immune response. Brain Behav Immun 26:623-634.
Patterson PH. 2011. Maternal infection and immune involvement in autism. Trends Mol Med 17:389-394.
Peleg-Raibstein D, Feldon J, Meyer U. 2012. Behavioral animal models of antipsychotic drug actions. Handb Exp Pharmacol:361-406.
Piontkewitz Y, Arad M, Weiner I. 2011. Abnormal trajectories of neurodevelopment and behavior following in utero insult in the rat. Biol Psychiatry 70:842-851.
Quarles RH. 2007. Myelin-associated glycoprotein (MAG): past, present and beyond. J Neurochem 100:1431-1448.
Richetto J, Calabrese F, Meyer U, Riva MA. 2013. Prenatal versus postnatal maternal factors in the development of infection-induced working memory impairments in mice. Brain Behav Immun 33:190-200.
Richetto J, Calabrese F, Riva MA, Meyer U. 2014. Prenatal immune activation induces maturation-dependent alterations in the prefrontal GABAergic transcriptome. Schizophr Bull 40:351-361.
Richetto J, Labouesse MA, Poe MM, Cook JM, Grace AA, Riva MA, Meyer U. 2015. Behavioral effects of the benzodiazepine-positive allosteric modulator SH-053-2'F-S-CH(3) in an immune-mediated neurodevelopmental disruption model. Int J Neuropsychopharmacol 18.
Richey JA, Damiano CR, Sabatino A, Rittenberg A, Petty C, Bizzell J, Voyvodic J, Heller AS, Coffman MC, Smoski M, Davidson RJ, Dichter GS. 2015. Neural Mechanisms of Emotion Regulation in Autism Spectrum Disorder. J Autism Dev Disord 45:3409-3423.
Samorajski T, Rolsten C. 1973. Age and regional differences in the chemical composition of brains of mice, monkeys and humans. Prog Brain Res 40:253-265.
Sanfilipo M, Lafargue T, Arena L, Rusinek H, Kushner K, Lautin A, Loneragan C, Vaid G, Rotrosen J, Wolkin A. 2000. Fine volumetric analysis of the cerebral ventricular system in schizophrenia: further evidence for multifocal mild to moderate enlargement. Schizophr Bull 26:201-216.
Sanfilipo M, Lafargue T, Rusinek H, Arena L, Loneragan C, Lautin A, Feiner D, Rotrosen J, Wolkin A. 2000. Volumetric measure of the frontal and temporal lobe regions in schizophrenia: relationship to negative symptoms. Arch Gen Psychiatry 57:471-480.
Schnaar RL, Lopez PH. 2009. Myelin-associated glycoprotein and its axonal receptors. J Neurosci Res 87:3267-3276.

Schubert D, Martens GJ, Kolk SM. 2015. Molecular underpinnings of prefrontal cortex development in rodents provide insights into the etiology of neurodevelopmental disorders. Mol Psychiatry 20:795-809.
Selemon LD, Zecevic N. 2015. Schizophrenia: a tale of two critical periods for prefrontal cortical development. Transl Psychiatry 5:e623.
Smith SE, Li J, Garbett K, Mirnics K, Patterson PH. 2007. Maternal immune activation alters fetal brain development through interleukin-6. J Neurosci 27:10695-10702.
Smith SM, Nichols TE. 2009. Threshold-free cluster enhancement: addressing problems of smoothing, threshold dependence and localisation in cluster inference. Neuroimage 44:83-98.
Suchiman HE, Slieker RC, Kremer D, Slagboom PE, Heijmans BT, Tobi EW. 2015. Design, measurement and processing of region-specific DNA methylation assays: the mass spectrometry-based method EpiTYPER. Front Genet 6:287.
Szyf M. 2015. Epigenetics, a key for unlocking complex CNS disorders? Therapeutic implications. Eur Neuropsychopharmacol 25:682-702.
Tang B, Jia H, Kast RJ, Thomas EA. 2013. Epigenetic changes at gene promoters in response to immune activation in utero. Brain Behav Immun 30:168-175.
Tebbenkamp AT, Willsey AJ, State MW, Sestan N. 2014. The developmental transcriptome of the human brain: implications for neurodevelopmental disorders. Curr Opin Neurol 27:149-156.
Vassall KA, Bamm VV, Harauz G. 2015. MyelStones: the executive roles of myelin basic protein in myelin assembly and destabilization in multiple sclerosis. Biochem J 472:17-32.
Vernon AC, Crum WR, Lerch JP, Chege W, Natesan S, Modo M, Cooper JD, Williams SC, Kapur S. 2014. Reduced cortical volume and elevated astrocyte density in rats chronically treated with antipsychotic drugs-linking magnetic resonance imaging findings to cellular pathology. Biol Psychiatry 75:982-990.
Wan C, Yang Y, Feng G, Gu N, Liu H, Zhu S, He L, Wang L. 2005. Polymorphisms of myelin-associated glycoprotein gene are associated with schizophrenia in the Chinese Han population. Neurosci Lett 388:126-131.
Winkler AM, Ridgway GR, Webster MA, Smith SM, Nichols TE. 2014. Permutation inference for the general linear model. Neuroimage 92:381-397.
Wong JH, Halliday GM, Kim WS. 2014. Exploring myelin dysfunction in multiple system atrophy. Exp Neurobiol 23:337-344.
Yang YF, Qin W, Shugart YY, He G, Liu XM, Zhou J, Zhao XZ, Chen Q, La YJ, Xu YF, Li XW, Gu NF, Feng GY, Song H, Wang P, He L. 2005. Possible association of the MAG locus with schizophrenia in a Chinese Han cohort of family trios. Schizophr Res 75:11-19.
Zai G, King N, Wigg K, Couto J, Wong GW, Honer WG, Barr CL, Kennedy JL. 2005. Genetic study of the myelin oligodendrocyte glycoprotein (MOG) gene in schizophrenia. Genes Brain Behav 4:2-9.

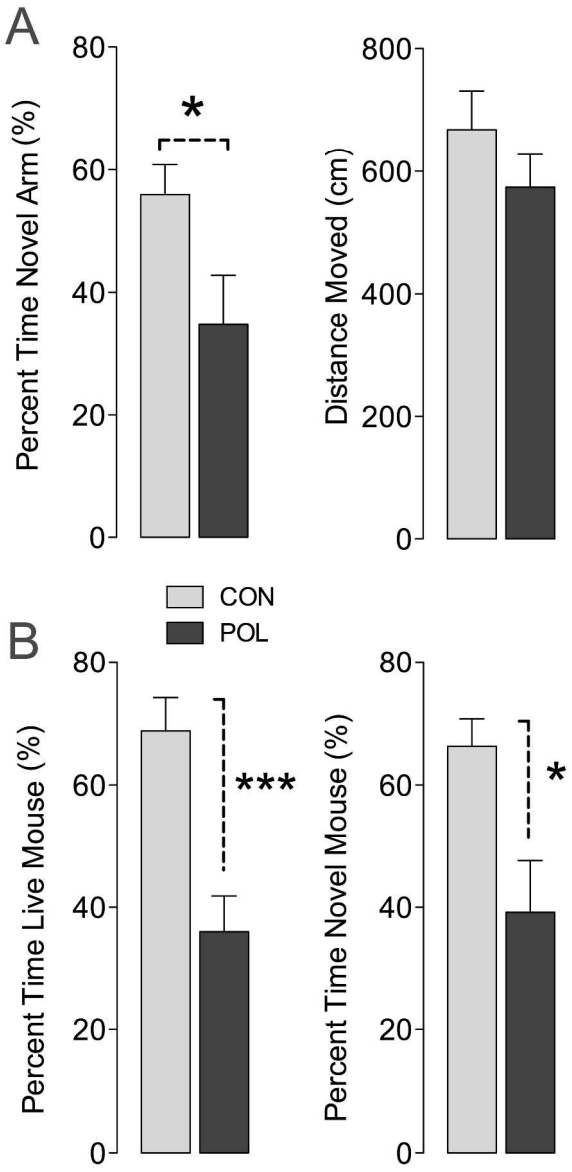

Figure 1. Cognitive and behavioral deficits following late prenatal immune activation. Mice were subjected to prenatal poly(I:C) treatment on gestation day 17 (POL), or they were exposed to prenatal control (CON) treatment. (A) Percent time spent in the novel arm during the Y-maze working memory test. *$p < 0.05$ based on independent Student's t tests (two-tailed). (B) Percent time spent with an unfamiliar live mouse, relative to an inanimate dummy object, during the social interaction test, and percent time spent with a novel live mouse, relative to a familiar one, during the social recognition test. *$p < 0.05$ and ***$p < 0.001$ based on independent Student's t tests (two-tailed). All data are based on N(CON) = 10, N(POL) = 10.
199x399mm (300 x 300 DPI)

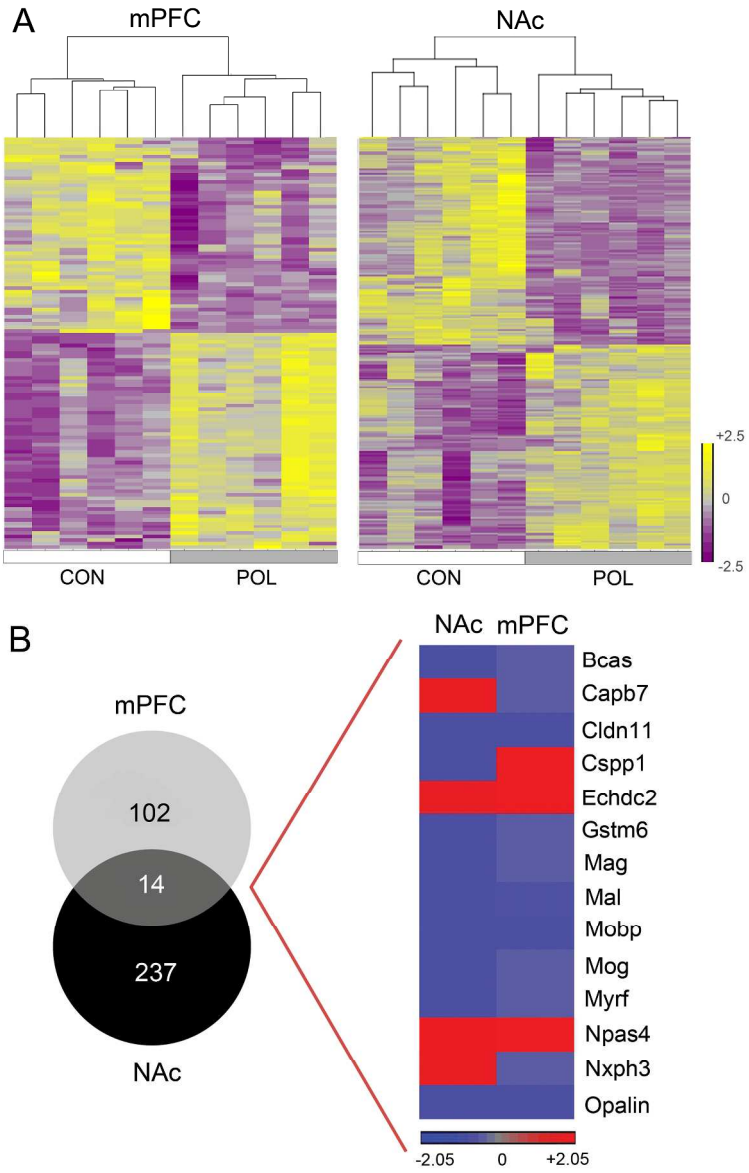

Figure 2. Unique and common gene expression differences following late prenatal immune activation in the mPFC and NAc, revealed by microarry. Mice were subjected to prenatal poly(I:C) treatment on gestation day 17 (POL), or they were exposed to prenatal control (CON) treatment. (A) Hierarchical clustering of differentially expressed genes in POL offspring relative to CON offspring in the mPFC and NAc. Down- and up-regulated genes are represented in purple and yellow color, respectively. (B) Venn Diagram depicting the number of genes that are uniquely and commonly affected in the mPFC and NAc of POL offspring. The commonly affected genes are listed, and down- and up-regulated genes are represented by blue and red color, respectively, in each brain area. All data are based on N(CON) = 6, N(POL) = 6.
290x454mm (300 x 300 DPI)

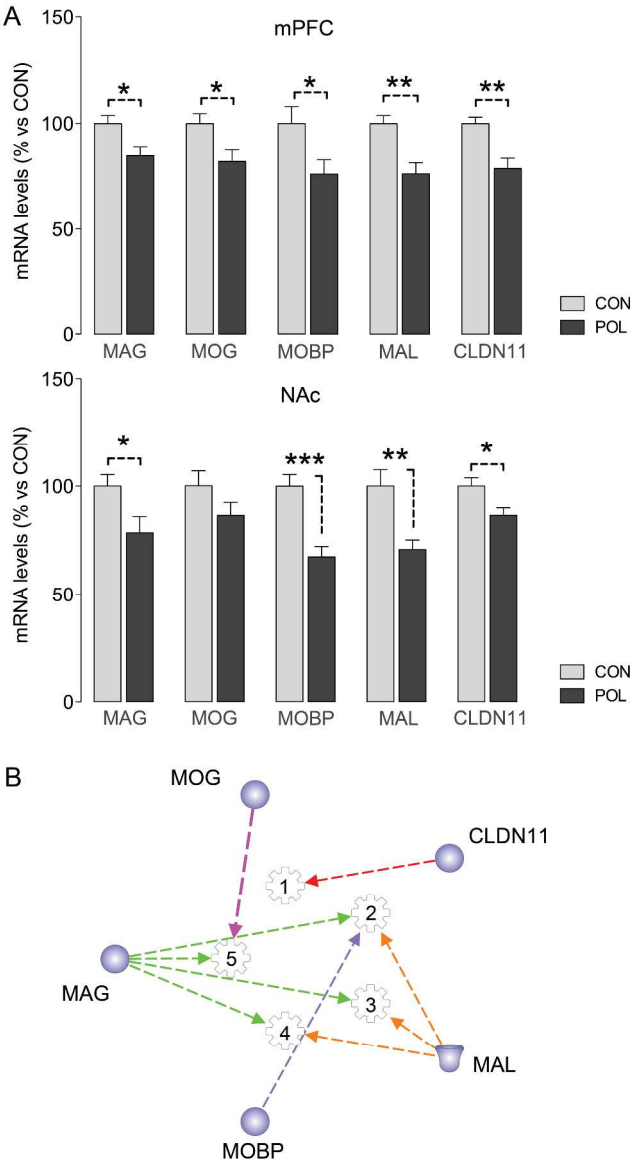

Figure 3. Validation of common myelin gene expression differences in the mPFC and NAc. Mice were subjected to prenatal poly(I:C) treatment on gestation day 17 (POL), or they were exposed to prenatal control (CON) treatment .(A) The bar plots represent the mRNA levels of each selected gene (% versus CON). The gene expression levels were assessed by RT-qPCR. *p < 0.05, **p < 0.01 and ***p < 0.001 based on independent Student's t tests (two-tailed). All data are based on N(CON) = 10, N(POL) = 10. (B) Graphical representation of the network analysis conducted on the commonly affected myelin genes. The analysis was conducted using Ingenuity Pathway Analysis (IPA), and each gene is represented in relation to the others and to the specific functions it is involved in. 1 = Ensheathment of axons; 2 = Myelination; 3 = Myelination of cells; 4 = Myelination of nerves; 5 = Dendritic growth and branching.
279x489mm (300 x 300 DPI)

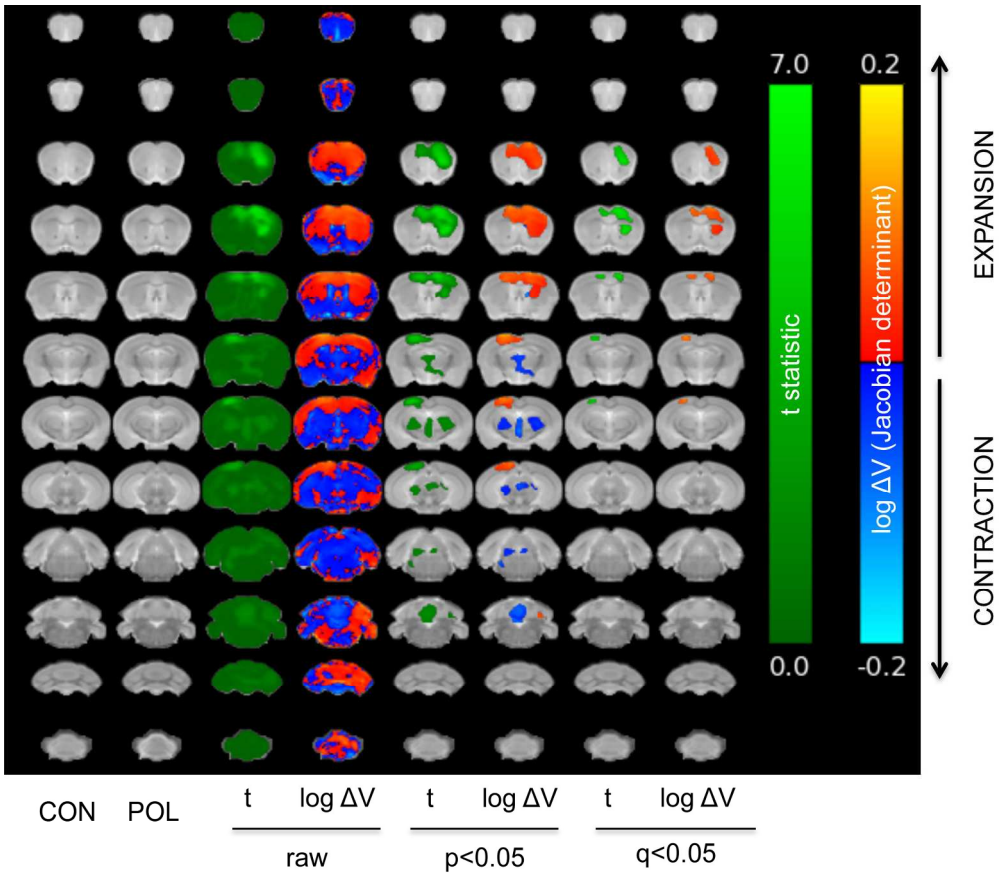

Figure 4. Alterations in neuroanatomy following late prenatal infection revealed by brain-wide tensor based morphometry analysis of 3D T2-weighted MR images. Mice were subjected to prenatal poly(I:C) treatment on gestation day 17 (POL), or they were exposed to prenatal control (CON) treatment. Data shown are raw values for log jacobian determinant and effect (t-statistic) thresholded at p<0.01 uncorrected and false discovery rate corrected at q<0.05.
189x165mm (300 x 300 DPI)

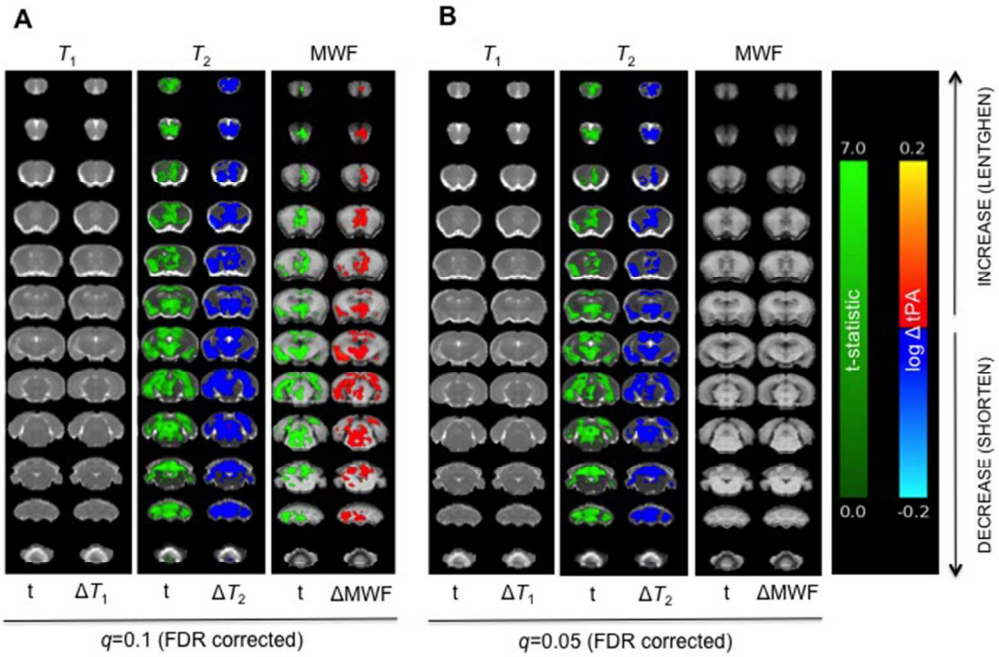

Figure 5. Alterations in T1, T2 relaxation time and myelin water fraction (MWF) following late prenatal infection as revealed by voxel-wise cluster analysis. Mice were subjected to prenatal poly(I:C) treatment on gestation day 17 (POL), or they were exposed to prenatal control (CON) treatment. Data shown for each parameter are the raw effects "t" (t-statistic) and significant voxel-wise changes in each tissue parameter relative to the control group thresholded at q<0.05 (False discovery rate corrected).
243x161mm (72 x 72 DPI)

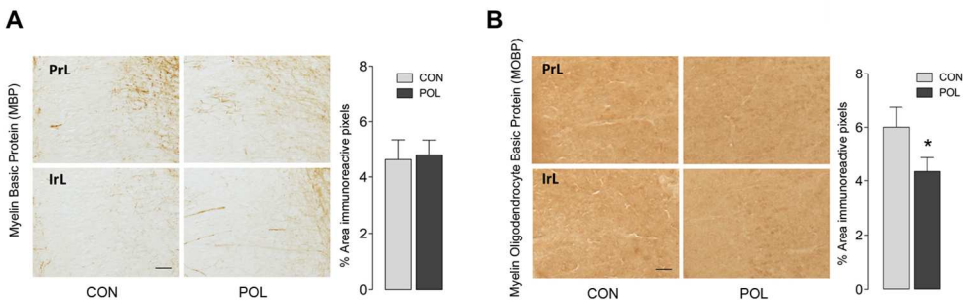

Figure 6. Protein expression alterations following late prenatal infection, as revealed by immunohistochemistry. Mice were subjected to prenatal poly(I:C) treatment on gestation day 17 (POL), or they were exposed to prenatal control (CON) treatment. (A) The bar plots represent the percent area of immunoreactive pixels for MBP. (B) The bar plots represent the percent area of immunoreactive pixels for MOBP. Representative photomicrographs of MBP and MOBP are presented in figure 6a and 6b, respectively at x4 magnifications, scale bar = 50 µm. ACC, anterior cingulate cortex; PrL, prelimbic cortex; Irl, infralimbic cortex. For MBP: N(CON) = 10, N(POL-) = 9; p=0.426, Cohens'd=0.088, Student's T-Test (one tailed). For MOBP: N(CON) = 7, N(POL) = 8; p=0.041, Cohens'd=0.961, Student's T-Test (one tailed).
260x85mm (150 x 150 DPI)

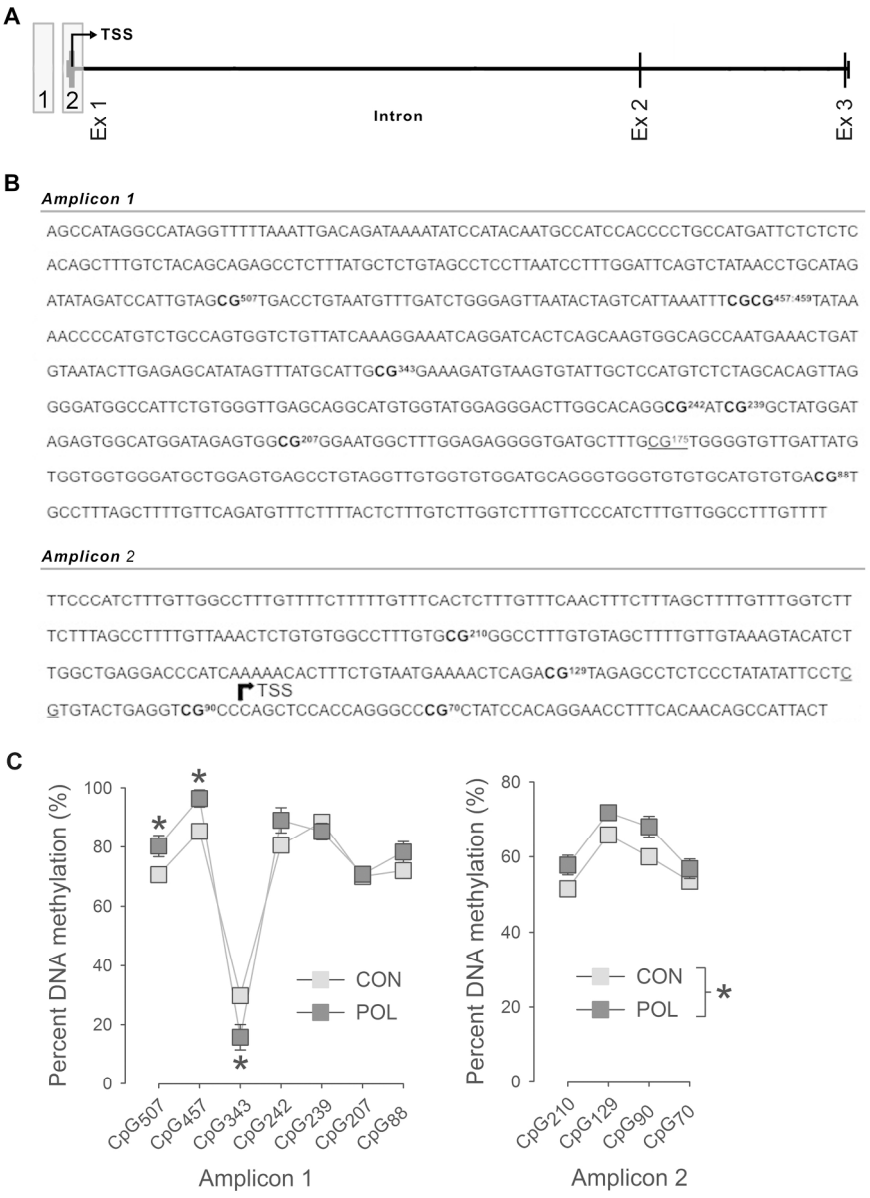

Figure 7. Investigation of DNA methylation differences in the promoter of the MOBP gene using EpiTYPER. Mice were subjected to prenatal poly(I:C) treatment on gestation day 17 (POL), or they were exposed to prenatal control (CON) treatment. (A) Graphical representation of the MOBP gene and genomic locations of the selected amplicons. (B) Sequences of the selected amplicons and position of investigated CpGs in each amplicon. Methylation of the numbered CpGs (in bold font) was accessible to quantification by EpiTYPER, whereas underlined CpGs were un-measurable for technical reasons. (C) Percent DNA methylation of specific CpGs in the selected amplicons. *p < 0.05, **p < 0.01, and ***p < 0.001, reflecting the significant differences between CON and POL offspring; based on post-hoc tests following the presence of a significant interaction between prenatal treatment and position in ANOVA (Amplicon 1: (F(6,54) = 5.35, p < 0.001 Amplicon 2: F(1,9) = 7.32, p < 0.05). N(CON) = 6, N(POL-) = 5.
193x266mm (300 x 300 DPI)

SUPPLEMENTARY INFORMATION

Genome-Wide Transcriptional Profiling and Structural Magnetic Resonance Imaging in the Maternal Immune Activation Model of Neurodevelopmental Disorders

Juliet Richetto[1,2,§], Robert Chesters[3,§], Annamaria Cattaneo[4,5], Ana Maria Carrillo Gutierrez[3], Tobias C. Wood[6], Alessia Luoni[7], Urs Meyer[1,2,*], Anthony Vernon[3,#], Marco A. Riva[7#]

[1]Institute of Pharmacology and Toxicology, University of Zurich-Vetsuisse, Zurich, Switzerland.
[2]Physiology and Behavior Laboratory, ETH Zurich, Schwerzenbach, Switzerland.
[3]Department of Basic and Clinical Neuroscience, Institute of Psychiatry Psychology and Neuroscience, King's College London, London, UK.
[4]Biological Psychiatry Laboratory, IRCCS Fatebenefratelli San Giovanni di Dio, Brescia, Italy.
[5]Stress, Psychiatry and Immunology Laboratory, Department of Psychological Medicine, Institute of Psychiatry, King's College London, London, UK.
[6]Department of Neuroimaging, Institute of Psychiatry Psychology and Neuroscience, King's College London, London, UK.
[7]Department of Pharmacological and Biomolecular Sciences, Università degli Studi di Milano, Milan, Italy.

[§]These authors corresponded equally to the present study.
[#]Shared seniority.

*Correspondence:
Urs Meyer, Ph.D.
Institute of Pharmacology and Toxicology
University of Zurich-Vetsuisse
Winterthurerstrasse 260,
8057 Zurich,
Switzerland

E-mail: urs.meyer@vetpharm.uzh.ch
Tel.: +41 44 635 88 44; Fax.: +41 44 635 89 10

Supplementary Materials and Methods

Working Memory Test

Working memory was assessed using a spatial recognition test in the Y-maze as established and validated before (Richetto J et al. 2013; Labouesse MA et al. 2015). This test uses the natural tendency of rodents to explore novel over familiar spatial environments. The apparatus was made of transparent Plexiglas and consisted of three identical arms (50 × 9 cm; length × width) surrounded by 10-cm high transparent Plexiglas walls. The three arms radiated from a central triangle (8 cm on each side) and were spaced 120° from each other. A removable opaque barrier wall was used to block access to each arm from the central area. The floor of the maze was covered with sawdust bedding, which was changed between sample and choice phases. The maze was elevated 90 cm above the floor and was positioned in a well-lit room enriched with distal spatial cues. A digital camera was mounted above the Y-maze apparatus. Images were captured at a rate of 5 Hz and transmitted to a PC running the EthoVision tracking system (Noldus Information Technology, The Netherlands), which calculated the time spent and distance moved in the three arms and center zone of the Y-maze.

The working memory test in the Y-maze consisted of two phases, called the sample and choice phases. The allocation of arms (start, familiar, and novel arm) to a specific spatial location was counterbalanced across the experimental conditions.

Sample phase: The animals were allowed to explore two arms (referred to as “start arm” and “familiar arm”). Access to the remaining arm (“novel arm”) was blocked by the opaque barrier wall. To begin a trial, the animal was introduced at the end of the start arm and was allowed to freely explore both the start and the familiar

arms for 5 min. Test timing was initiated once the subject had made an entry into the central triangular area, as detected by the EthoVision tracking system. The animal was then removed and kept in a holding cage prior to commencement of the choice phase. The barrier door was removed and the sawdust flooring changed to avoid olfactory cues.

Choice phase: The animal was introduced to the maze following a retention interval of 1 min. During the choice phase, the barrier wall was removed so that the animals could freely explore all arms of the maze for 2 min. The animal was then removed from the maze and returned to the home cage. The sawdust flooring was changed in preparation for the next trial.

On each trial, the time spent in each of the three arms was recorded. The relative time spent in the novel arm during the choice phase was calculated by the formula ([time spent in the novel arm]/[time spent in all arms]) × 100 and used as the index for short-term spatial recognition memory. In addition, total distance moved on the entire maze was recorded and analyzed in order to assess general locomotor activity.

Social Interaction and Recognition Test

The apparatus was made of opaque Plexiglas and consisted of three identical arms (50 × 9 cm; length × width) surrounded by 10-cm high Plexiglas walls. The three arms radiated from a central triangle (8 cm on each side) and were spaced 120° from each other. The floor of the maze was covered with sawdust bedding, which was changed between each individual habituation and test trial. Two of the three arms contained rectangular wire grid cages (13 × 8 × 10 cm, length × width × height; bars horizontally and vertically spaced 9 mm apart). The third arm did not contain a metal wire cage and served as the start zone (see below). The apparatus was located in an

experimental testing room under dim diffused lighting (~35 lux as measured in the individual arms).

The test of social interaction consisted of two phases, namely the 'dummy phase' and the 'novelty phase', which indexes social approach behavior and social recognition, respectively (Richetto J et al. 2015). The allocation of arms (start, familiar and novel arm) to a specific spatial location was counterbalanced across experimental groups.

• *Dummy phase:* The animals were allowed to explore the three arms (referred to as 'start arm', 'dummy arm' and 'live arm'). During this phase, one metal wire cage contained an unfamiliar C57BL6/N mouse ('live mouse'), and the other wire cage contained an inanimate object ('dummy mouse'), which was made of black LEGO™ (Billund, Denmark) bricks and took the shape of a mouse. To begin a trial, the animal was introduced at the end of the start arm and was allowed to freely explore all three arms for 5 min. Behavioral observations were made by an experimenter who was blind to the experimental conditions. Social interaction was defined as nose contact within a 2-cm interaction zone. The percent time spent with the live mouse was calculated by the formula (time spent with the live mouse/(time spent with the live mouse + time spent with the dummy object)) × 100 and used to assess relative exploration time between a congenic mouse and an inanimate dummy object. On completion of the 'dummy phase', the animal was removed and kept in a holding cage, during which the sawdust flooring was changed to avoid olfactory cues.

• Novelty phase: Another unfamiliar C57BL6/N mouse, which is referred to as the 'novel mouse' during the second phase of the test, now replaced the inanimate dummy mouse. The other cage contained the 'familiar mouse' previously used in the 'dummy phase'. The allocation of the 'novel mouse' and 'familiar mouse' to the two wire cages was counterbalanced across experimental groups. To start the 'novelty

phase', the animal was introduced into the maze again and was allowed to freely explore all three arms for 5 min. Behavioral observations for social interaction were scored as described before. The percent time spent with the novel mouse was calculated by the formula (time spent with the novel mouse/(time spent with the novel mouse + time spent with the familiar mouse)) × 100 and used to assess relative exploration time between the familiar and unfamiliar congenic mouse.

DNA and RNA Isolation and Quantitative Real-Time PCR Analyses

Total DNA and RNA were isolated using the Qiagen AllPrep DNA and RNA Mini kit (Qiagen, Italy) according to the manufacturer's instructions, and quantified by spectrophotometric analysis. An aliquot of each RNA sample was then treated with DNase to avoid DNA contamination. RNA was analysed by TaqMan qRT-PCR instrument (CFX384 real-time system, Bio-Rad Laboratories) using the iScript one-step RT-PCR kit for probes (Bio-Rad Laboratories). The samples were run in 384-well formats in triplicates as multiplexed reactions with a normalizing internal control (36B4). We choose 36B4 as internal standard for gene expression analyses since its expression was not affected by prenatal treatment and further manipulations.

Thermal cycling was initiated with an incubation at 50°C for 10 min (RNA retrotranscription) and then at 95°C for 5 min (TaqMan polymerase activation). After this initial step, 39 cycles of PCR were performed. Each PCR cycle consisted of heating the samples at 95°C for 10 s to enable the melting process and then for 30 s at 60°C for the annealing and extension reaction. Relative target gene expression was calculated according to the 2(-Delta Delta C(T)) method (Livak KJ and TD Schmittgen 2001). Probe and primer sequences of Claudin11 (Assay: Mm00500915_m1) were purchased from Life Technologies (Switzerland), while the custom designed probe and primer sequences used for MOBP, MOG, MAL and MAG

are summarized in **Supplementary Table 1** and were purchased from Eurofins Genomics GmbH (Germany).

Gene	Forward Primer	Reverse Primer	Probe
MOBP	5'-TTCTTCGAGGATGGGTGCAT-3'	5'-AGCAGCTCACACGTACAAGA-3'	5'-CACCATTTCTTCCTCCTGTTCC-3'
MAG	5'-CCTTCAACCTGTCTGTGGAGTT-3'	5'-CGGGTTGGATTTTACCACAC-3'	5'-CCCATAATCCTTCTGGAGTCAC-3'
MOG	5'-CTCCATCGGACTTTTGATCC-3'	5'-AGCAGATGATCAAGGCAACC-3'	5'-ATTGTGCCTGTTCTTGGACC-3'
MAL	5'-CGTGGTCCATGCTGTGTTTT-3'	5'-TTTCTCCACCATCCAGTCTGTG-3'	5'-GCCCATCTTCCCCATTAACTTC-3'
36B4	5'-AGATGCAGCAGATCCGCAT-3'	5'-GTTCTTGCCCATCAGCACC-3'	5'-CGCTCCGAGGGAAGGCCG-3'

Microarray Analyses

Gene expression microarray assays were performed using Mouse Gene 1.1 ST Array Strips on GeneAtlas platform (Affymetrix), following the 3'IVT one cycle labeling and amplification protocol described in the Affymetrix GeneChip Expression Analysis Technical Manuals and in the GeneAtlas™ WT Expression Kit User Manual. Mouse Gene 1.1 ST Array Strips are comprised of more than 530,000 probes covering more than 36,000 transcripts and variants, which represent more than 20,000 genes mapped through UniGene or via RefSeq annotation.

To synthesize First-Strand cDNA, 250ng RNA were reverse-transcribed with the Gene Atlas 3'IVT Express Kit or WT Expression Kit (Affymetrix, Santa Clara, CA, USA) using T7 oligo(dT) primer. Second-Strand cDNA synthesis was carried out using DNA polymerase and RNase H to simultaneously degrade RNA and synthesize second-strand cDNA. This step was followed by the in vitro transcription using IVT Labelling Master Mix to generate multiple copies of biotin-modified antisense-RNA (aRNA) from the double-stranded cDNA templates. Subsequently strand DNA was purified to remove unincorporated NTPs, salts, enzymes and inorganic phosphate. Labelled cDNA (10ug) was then fragmented and 7.5µg were hybridized onto Mouse

Gene 1.1 ST Array Strips. The reactions of hybridation, fluidics and imaging were performed on the Affymetrix Gene Atlas instrument according to the manufacturer's protocol.

DNA Methylation Analysis

Promoter methylation analysis of MOBP was performed using the EpiTYPER assay for the detection and quantitative analysis of DNA methylation using base-specific cleavage and Matrix-Assisted Laser Desorption/Ionization Time-of-Flight Mass Spectrometry (MALDI-TOF MS). Genomic DNA was treated and analysed according to manufacturers' instructions (Agena Bioscience). Briefly, genomic DNA was treated with bisulfite and amplified by PCR with primers specific to the MOBP promoter (Table 2) under these cycling conditions: 95°C for 2', followed by 49 repeated cycles (95.0°C for 40'', 56.0°C for 40'', 72.0°C for 40'') and a last step at 72.0 °C for 5'00''.

Unincorporated dNTPs leftover from amplification were neutralized using shrimp alkaline phosphatase (SAP). Then, to obtain fragmented RNA molecules, in-vitro RNA transcription with subsequent base specific cleavage using RNase A was performed. Both methylated and nonmethylated regions were cleaved at every T to produce fragments that are identical in length and differ only in their nucleotide composition. The samples were then conditioned so that the products could be processed in the MALDI-TOF mass spectrometer and could be analysed by their mass spectra. In analysing the mass spectrum, the relative amount of methylation can be calculated by comparing the difference in signal intensity between mass signals derived from methylated and nonmethylated template DNA.

The primer sequences used to amplify specific genomic regions (amplicons 1-2, A1-2) of the MOBP gene were as follows:

Amplicon	Forward Primer (bold letters: gene specific)	Reverse Primer (bold letters: gene specific)
A1	5'-aggaagagagAAAATAAAGGTTAATAAAGATGGGAA -3'	5'-gggagaaggctAACCTCCTTAATCCTTTAAATTCAATC -3'
A2	5'-aggaagagagGGGTGAATTAGAGTTTTGGAATTTT -3'	5'-gggagaaggctTTCCCATCTTTATTAACCTTTATTTTC -3'

MRI acquisition

A 7T horizontal small bore magnet and (Agilent Technologies Inc. Santa Clara, USA) and a quadrature volume radiofrequency coil (39 mm internal diameter, Rapid Biomedical GmbH) were used for all MRI acquisition. Fixed brain samples were placed securely up to four at a time in a custom-made MR-compatible holder and immersed in proton-free susceptibility matching fluid (FluorinertTM FC-70; Sigma-Aldrich, UK). Samples were scanned in a random order.

The following MR images were acquired: T_2-weighted 3D Fast Spin-Echo (FSE) and a multi-component Driven Equilibrium Single Pulse Observation of T_1 and T_2 (mcDEPSOT) protocol with B1 correction. The latter consists of a Spoiled Gradient echo (SPGR), balanced Steady State Free Procession (bSSFP) and Actual Flip-angle imaging (AFI) scans (Deoni SC et al. 2013). The mcDESPOT protocol generates data to calculate parametric maps of T_1, T_2 and the myelin water fraction (MWF) for each animal (**Supplementary Figure 1**). Parameters for each scan are summarised in **Supplementary Table 3**.

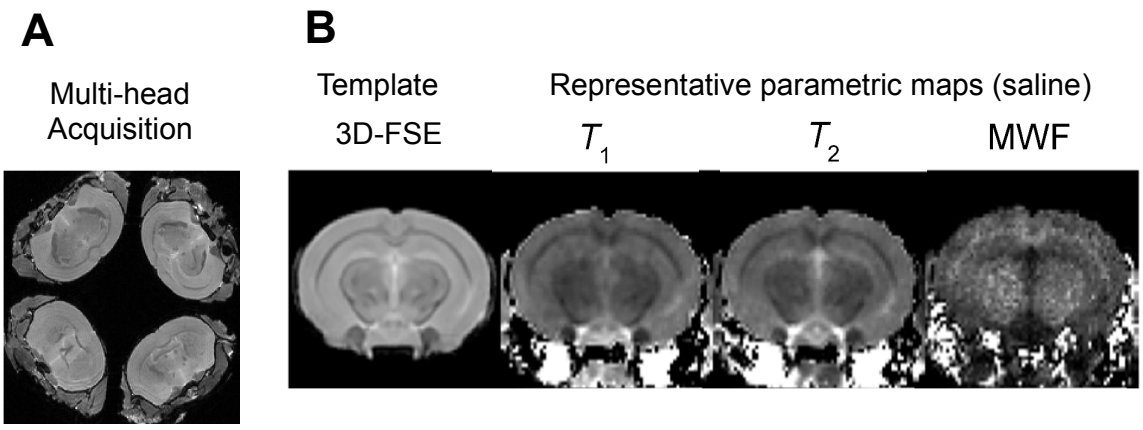

Supplementary Figure 1

Scan	Matrix size	FOV (mm)	Voxel size (μm^3)	T_R/T_E (ms)	Flip angles (°)	Scan duration
3D-FSE	256 x256x256	28.8x28.8x28.8	112.5	3000/40	-	3hrs 25min
SPGR	192x192x192	28.8x28.8x28.8	150	20/5.1	4,5,6,8,10,12,16,20,25,26,28,30	2hrs 27min
bSSFP	192x192x192	28.8x28.8x28.8	150	6/3	8,9,10,12,15,20,30,40,50,55,60,65	2hrs 56min
AFI	96x96x96	28.8x28.8x28.8	300	20/4.3	55	40mins

Supplementary Table 3. Scan Parameters. FSE- Fast Spin-Echo, SPGR - Spoiled GRadient echo, bSSFP – balanced Steady-State Free Precession, AFI - Actual Flip-angle Imaging. The bSSFP scan had 4 phase-cycling patterns (0, 90, 180, 270). The 3D FSE scan used 16 echoes spaced by 6.67ms.

MR image processing and analysis

The multi-head scans were split into individual sample by identifying the four largest connected-components, calculating their centre-of-gravity (CoG) and applying a rigid transform that moved the CoG to the origin and rotated the scans about the z-axis so that they were aligned correctly. These images were then visually inspected for any anomalies. No anatomical scans were excluded on this basis. However, due to the presence of image intensity and ghosting artefacts, the T_1, T_2 and MWF maps from 4

CON animals and 2 POL animals, respectively, were excluded. The final data set for analysis was therefore: *N*(CON)=10 and *N*(POL)=10 for 3D-FSE anatomical scans, and *N*(CON)=6 and *N*(POL)=8 for the T_1, T_2 and MWF.

In post-processing, the SPGR and bSSFP scans were smoothed with a Gaussian kernel (σ =200μm) to improve signal to noise ratio (SNR) for mcDESPOT fitting. The AFI scans were used to calculate B1 inhomogeneity (Yarnykh VL 2007). The T_1, T_2 and MWF maps were then calculated using our open-source C++ software (github.com/spinicist/QUIT). T_1 maps were calculated using a Weighted Least-Squares formulation of DESPOT1 (Chang LC et al. 2008). T_2 maps were calculated using the DESPOT2-FM method (Deoni SC 2009), MWF maps were calculated using a three-pool version of mcDESPOT (Deoni SC *et al.* 2013). A study template was then built from the individual 3D FSE structural images (*N*=20) using a population-based registration method based on FSL-FLIRT (Jenkinson M and S Smith 2001; Jenkinson M et al. 2002; Crum WR et al. 2013) Briefly, the images were registered together through a process of linear (9 degrees of freedom) and nonlinear registration to allow calculation of an average image of all the scans, yielding deformation fields for each individual brain. Subsequently, these displacement fields, containing the local deformations relative to the template, were applied to re-orient the calculated parametric maps of T_1, T_2 and MWF for each individual animal into the template space.

To measure group-level differences (CON versus POL) in neuroanatomy, the log-transformed Jacobian determinants of the deformation fields were then calculated for each 3D-FSE image, providing an estimate of local volume expansion/contraction at every voxel in the brain, using tensor based morphometry (TBM) as described previously (Vernon AC et al. 2014). The Jacobian determinant ranges from 0 (100% shrinkage) over 1 (no volume change) without any upper boundary (volume

increase). A logarithmic transform renders the Jacobian distribution symmetric, setting aside *a priori* assumptions on volume growth (Hammelrath L et al. 2016). Group-level differences in MRI parameters (volume, T_1, T_2 and MWF) between control and polyI:C offspring were analysed voxel-wise across the whole-brain using permutation testing and threshold free cluster enhancement (TFCE) (Smith SM and TE Nichols 2009; Winkler AM et al. 2014) at an uncorrected *p* value of 0.01. Multiple comparisons were controlled for using the false discovery rate (FDR) (Genovese CR et al. 2002) at $q = 0.05$.

Immunohistochemistry

After completion of all MR imaging, fixed brain tissues were dissected from the skull, hemisected and incubated in 4% PFA / 0.01M PBS for 24 hours, followed by cryoprotection in 30% buffered sucrose solution for 72 hours at +4°C. Coronal brain sections (40 µm-thick) were cut from the right hemisphere on a freezing microtome (-20°C) and collected into an individual well of a 96-well plate containing tissue cryoprotection solution (TCS: 25% glycerin [vol/vol] 30% ethylene glycol [vol/vol] in 0.2 mol/L phosphate buffer + 0.05% sodium azide), stored at +4°C.

For immunohistochemical staining, a 1 in 6 series of free-floating brain tissue sections from each animal were rinsed in PBS (3 x 5 minutes), followed by 1% H_2O_2 in PBS to block endogenous peroxidase activity (30 minutes). Blocking of non-specific binding was performed using 15% normal goat serum (NGS) (MP Biomedicals GmbH, Eschwege, Germany) diluted in PBST (0.1M PBS + 0.1%Triton-X100) (2 hours) at room temperature. The following primary antibodies were used: Rabbit α-Myelin Basic Protein (MBP; Abcam, Cat no. ab7349; diluted 1:1000) and rabbit α-Myelin-associated Oligodendrocytic Basic Protein (MOBP; Abcam, Cat no. ab203388; diluted 1:500). All antibodies were diluted in PBS containing 0.1% Triton

X-100 and 10% NGS, and sections were incubated free-floating overnight at +4°C. After PBS washes (3 x 5 minutes) sections were incubated for 1 hour with biotinylated goat α-rabbit secondary antibodies, diluted 1:1000 in PBS. Sections were washed again in PBS (3 x 5 minutes) and incubated with Vectastain ELITE ABC kit (Vector Laboratories, Burlingame CA, USA) for 1 hour at room temperature. After three washes in PBS (5 minutes), sections were stained using a 3'3-diaminobenzidine (DAB) peroxidase (HRP) staining kit (Vector laboratories, Inc. Burlingame, CA) for precisely 5 minutes to ensure consistent exposure, followed by four rinses in ice-cold PBS, dehydration and coverslipping with DPX (Sigma-Aldrich, UK).

Threshold Image Analysis for Myelin Staining

Quantitative analyses of MBP and MOBP-positive staining were performed in the prefrontal cortex using unbiased threshold image analysis. Briefly, a contour was drawn around the region of interest in each section at low magnification (x2.5) using an Olympus microscope with charge-coupled device camera and XYZ motorized specimen stage (Olympus UK Ltd., Southend-on-Sea, Essex, United Kingdom) connected to a personal computer running Stereo investigator software v7.0 (MBF BioScience, Williston, Vermont). Non-overlapping images were acquired from prefrontal cortex (x20 magnification n=12 images per animal across 4 consecutive sections corresponding to bregma +2.34 to +1.34 mm) using the meander function in StereoInvestigator software. These images were transformed off-line into binary images using the "make binary" tool implemented into ImageJ software (version 1.46r, NIH, Bethesda, MD, USA) without applying supplementary thresholds. Dark-brown areas were defined as "stained for myelin" (Hammelrath L *et al.* 2016). All post-processing and analysis was performed using ImageJ software. To calculate the

percentage area of pixels immunoreactive for either MBP or MOBP per region, per animal, the percentage area of positive pixels from each Individual image in a given ROS across all 4 consecutive sections were averaged to give a single value or the area of positive pixels per region per animal.

References

Chang LC, Koay CG, Basser PJ, Pierpaoli C. 2008. Linear least-squares method for unbiased estimation of T1 from SPGR signals. Magn Reson Med 60:496-501.

Crum WR, Giampietro VP, Smith EJ, Gorenkova N, Stroemer RP, Modo M. 2013. A comparison of automated anatomical-behavioural mapping methods in a rodent model of stroke. J Neurosci Methods 218:170-183.

Deoni SC. 2009. Transverse relaxation time (T2) mapping in the brain with off-resonance correction using phase-cycled steady-state free precession imaging. J Magn Reson Imaging 30:411-417.

Deoni SC, Matthews L, Kolind SH. 2013. One component? Two components? Three? The effect of including a nonexchanging "free" water component in multicomponent driven equilibrium single pulse observation of T1 and T2. Magn Reson Med 70:147-154.

Genovese CR, Lazar NA, Nichols T. 2002. Thresholding of statistical maps in functional neuroimaging using the false discovery rate. Neuroimage 15:870-878.

Hammelrath L, Skokic S, Khmelinskii A, Hess A, van der Knaap N, Staring M, Lelieveldt BP, Wiedermann D, Hoehn M. 2016. Morphological maturation of the mouse brain: An in vivo MRI and histology investigation. Neuroimage 125:144-152.

Jenkinson M, Bannister P, Brady M, Smith S. 2002. Improved optimization for the robust and accurate linear registration and motion correction of brain images. Neuroimage 17:825-841.

Jenkinson M, Smith S. 2001. A global optimisation method for robust affine registration of brain images. Med Image Anal 5:143-156.

Labouesse MA, Dong E, Grayson DR, Guidotti A, Meyer U. 2015. Maternal immune activation induces GAD1 and GAD2 promoter remodeling in the offspring prefrontal cortex. Epigenetics 10:1143-1155.

Livak KJ, Schmittgen TD. 2001. Analysis of relative gene expression data using real-time quantitative PCR and the 2(-Delta Delta C(T)) Method. Methods 25:402-408.

Richetto J, Calabrese F, Meyer U, Riva MA. 2013. Prenatal versus postnatal maternal factors in the development of infection-induced working memory impairments in mice. Brain Behav Immun 33:190-200.

Richetto J, Labouesse MA, Poe MM, Cook JM, Grace AA, Riva MA, Meyer U. 2015. Behavioral effects of the benzodiazepine-positive allosteric modulator SH-053-2'F-S-CH(3) in an immune-mediated neurodevelopmental disruption model. Int J Neuropsychopharmacol 18.

Smith SM, Nichols TE. 2009. Threshold-free cluster enhancement: addressing problems of smoothing, threshold dependence and localisation in cluster inference. Neuroimage 44:83-98.

Vernon AC, Crum WR, Lerch JP, Chege W, Natesan S, Modo M, Cooper JD, Williams SC, Kapur S. 2014. Reduced cortical volume and elevated astrocyte density in rats chronically treated with antipsychotic drugs-linking magnetic resonance imaging findings to cellular pathology. Biol Psychiatry 75:982-990.

Winkler AM, Ridgway GR, Webster MA, Smith SM, Nichols TE. 2014. Permutation inference for the general linear model. Neuroimage 92:381-397.

Yarnykh VL. 2007. Actual flip-angle imaging in the pulsed steady state: a method for rapid three-dimensional mapping of the transmitted radiofrequency field. Magn Reson Med 57:192-200.